Noise cancellation by cross–triggering Scintillating Fiber Beam Monitors in the CERN Experimental Areas

REGENSBURG

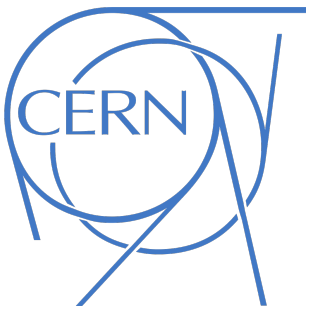

Bachelor's thesis presented in August 2018
at the Faculty of Electrical Engineering
and Information Technology of the
Technical University of Applied Sciences Regensburg
submitted by

Matthias Raudonis

in partial fulfillment of the requirements for the degree

Bachelor of Engineering (B.Eng.)

supervised by

Martin Schubert, OTH Regensburg

Inaki Ortega Ruiz, CERN Beam Instrumentation

Gerard Tranquille, CERN Beam Instrumentation

Geneva, 2018
Version 2.0

CERN-THESIS-2018-233
26/08/2018

Abstract

At CERN in Switzerland, particles are being accelerated by alternating electric current and forced on circular trajectories by dipole magnets in synchrotrons. In the CERN Experimental Areas, the Beam Instrumentation Group (BEAMS-BI) is working on a new particle detector for low-intensity secondary beams, including the beamline to the novel CERN Neutrino Platform. This XBPF Scintillating Fiber (SciFi) particle detector can detect individual particles and create a beam profile within an active area of 192 x 192 mm. The scintillation is detected by Silicon Photomultipliers (SiPM), connected to application specific readout electronics. The reverse-biased SiPM additionally output false signals generated from thermal noise (Dark Count Events, DCE), which need to be filtered.
The detected Dark Count Rate (DCR) can be lowered by increasing the detection threshold, with a reduction of detection efficiency. By creating a logical AND coincidence between two detectors, the detector planes can cross-trigger, which significantly reduces the DCR thermal noise. To create the AND coincidence, both XBPF Frontend and VFC Backend FPGAs need to be reprogrammed and tested. The resulting particle detector is evaluated and compared to existing systems.

The hardware updates were implemented on Xilinx and Intel FPGAs. Over a course of two month, data from cosmic muons was acquired by the testbench in different settings. A data analysis framework based on ROOT, Python and shell scripts was created to visualize and analyse the dataset. To further investigate the efficiency of the cross trigger configuration, a virtual cross trigger was created. This virtual trigger and the new modes were validated by data analysis.
The data analysis of beam profiles, noise measurements, efficiency measurements, oscilloscope measurements, angular profiles and continuity analysis methods verified the function of the new trigger modes and the channels masking feature.

The Cross Trigger performs very well in noise cancellation and efficiency comparisons. At the desired threshold of 290, the thermal noise is cancelled while the combined detection efficiency is higher than with the External Trigger.

The new detectors are currently (2018) in operation in the new EHN 1 Extention H2 of the SPS north hall in CERN.

Contents

List of Figures

List of Tables

Listings

List of abbreviations

Acronym	Word
SciFi	Scintillating Fiber
FMC	FPGA Mezzanine Card
SiPM	Silicon Photomultiplier
ASIC	Application-specific Integrated Circuit
SNR	Signal-to-noise Ratio
MPPC	Multi-Pixel Photon Counter
XBPF	X Beam Profile Monitor
CERN	Conseil Européen pour la Recherche Nucléaire
G-APD	Geiger-Mode Avalanche Photodiode
VME	Versa Module Europa
VFC	VME FMC Carrier
FMC	FPGA Mezzanine Card
RF	Radio Frequency
PLL	Phase-locked loop
CDR	Clock Data Recovery
DCE	Dark Count Event
DCR	Dark Count Rate
ET	External Trigger
ST	Self Trigger
CT	Cross Trigger
VCT	Virtual Cross Trigger
VLI	Very Low Itensity

Table 1 – List of Acronyms

1 Motivation

This thesis is the outcome of my education from the University of Applied Sciences Regensburg and a six–months trainee-ship at the European Organization for Nuclear Research (CERN).

From time immemorial, mankind was striving for the answers of two very basic questions:

- **What are we made of?**
- **What is out there?**

Thousands of years of scientific progress in the fields of biology, physics, chemistry and astronomy define our modern world and how we see it.
Yet, the full answers of these basic questions are still to be found. The Standard Model is a good description of the subatomic world but fails to explain the complete picture. Because of the limitation of the observable universe, modern astronomy also fails to find a complete answer to the second question.

Ironically, looking at collisions of particles that are small beyond human imagination can help us understand our universe, which is big beyond human imagination.

Even though our remarkable knowledge of our modern world, we still might not know what 95% of the universe is made of. [1] I hope one day mankind will find the answers to these questions and develop to know more than a dog looking at the moon.

[1] Dark Matter and Dark Energy theories

2 Beam Monitoring Systems

To measure the properties like the numbers of particles, the length and profile of bunches and also individual particles, the XBPF contains following systems.

2.1 Scintillating Fibers

To detect particles in the past, wire and bubble chambers were favorized. Due to the advance in microelectronics and Silicon Photomultipliers (section 2.2), Scintillating Fibers are rediscovered for particle detection.

Scintillating Fibers are plastic fibers, designed for trapping and transmitting light. The core of the fiber is typically made of Polystyrene, which emits photons upon interaction with energetic particles. A fluorescent dye is added to shift the interaction wavelength to the desired transportation wavelength. The emitted photons are captured by total internal reflection and transported to the ends of the fiber. [1] The used Scintillating Fibers have a size of 1 x 1 mm and peak at a wavelength of 450 nm (blue). Additionally, they are coated with aluminium to prevent optical crosstalk between the fibers. A mirror at the non - detector facing end of the fiber theoretically doubles the number of photons arriving at the detector.

2.2 Silicon photomultipliers

To detect the photons captured and transported by the fiber, Silicon Photomultipliers were chosen over the other considered technologies, including Avalanche Photodiodes (APD), Charge-Couple Devices (CCD), Hybrid Photodiodes (HPD), Photomultiplier Tubes (PMT), Position Sensitive Photomultipliers and Multi-Anode Photomultiplier Tubes (MA-PMT). For the XBPF Frontend Board the MPPC S13360-1350CS from Hamamatsu Photonics were chosen for their low crosstalk and DCR (Dark Count Rate) of 26.3 ± 4.2 kHz. [2] The S13360-1350C MPPC has 667 pixels with a pixel pitch of $50\mu m$ on a photosensitive area of 1.3 x 1.3 mm. [3]

2.2.1 Function and Layout

Geiger-Mode Avalanche Photodiode (G-APD)

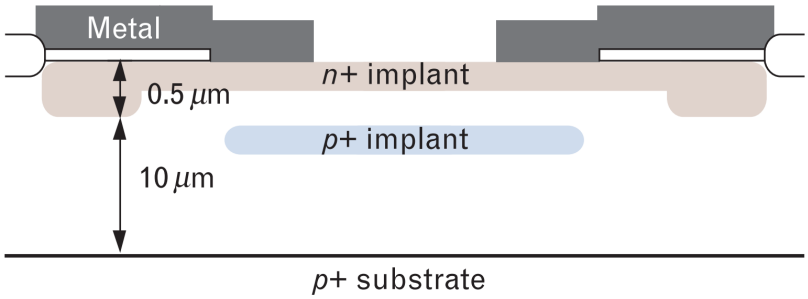

Figure 2.1 – Lateral cut of a Geiger-Mode Avalanche Photodiode [4]

A Geiger-Mode Avalanche Photodiode (G-APD) is a semiconducting photodiode, working with a reverse-biased p-n junction. The depletion region is comparably thick to avoid electron tunnelling, which leads to an unwanted Zener-Breakdown. (see figure 2.1)

$$V_A < V_B \qquad \text{Insulation, } I_{pn} = 0 \tag{2.1}$$

$$V_A > V_B \qquad \text{Avalanche breakdown possible} \tag{2.2}$$

If the voltage of the diode V_A is set above the breakdown voltage V_B, the diode may start conducting in reverse. (State 2.2) To start this process, a single charge carrier (electron or hole) in the p-n junction is sufficient. This carrier is accelerated by the strong electric field E_{pn} and will create new electron-hole pairs by collision and breaking of other covalent bonds. These new charge carriers are also accelerated by the electric field E_{pn}. [5] This leads to an avalanche effect, which immediately multiplies the number of pairs by a factor of 10^6 to 10^7. [2] This leads to a sub-nanosecond rise-time of the current until it is limited to a steady level by a serial quenching resistor R_Q.

The charge carrier causing the avalanche is created by an incoming photon passing the depletion layer. The time of the photon arriving can be determined at the beginning of the steep current rise. An other unwanted source of ionizing charge carriers is thermal noise, which is further discussed in section 2.2.3.

To set the diode back to an idle state to allow new photon detections, the reverse diode voltage V_A has to be lowered below the breakdown voltage V_B to stop the current. (State 2.1) Setting the voltage above the breakdown voltage V_B enables the diode to breakdown and detect again. (State 2.2) [2]

SiPM Photodiode Matrix

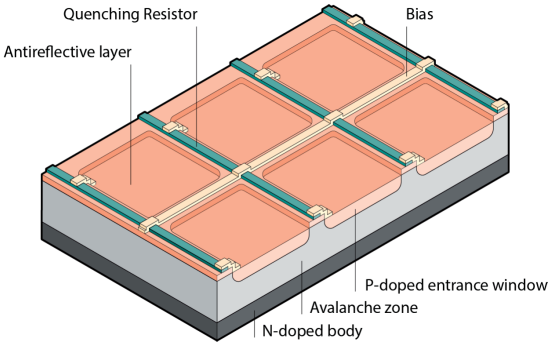

Figure 2.2 – MPPC SiPM layout [2]

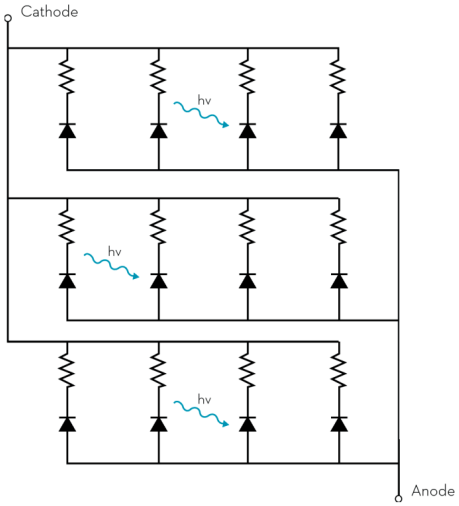

Figure 2.3 – MPPC SiPM schematic [2]

Silicon Photomultipliers (SiPM), also known as Multi-Pixel Photon Counter (MPPC) are a new semiconductor, using a matrix of multiple G-APD on the same silicon substrate. (see figure 2.2) This improves the size, efficiency and binary limitations of the G-APD. The chosen SiPM S13360-1350C for this purpose has 667 G-APD pixels. By placing multiple parallel G-APD and quenching resistor pairs in parallel, (figure 2.3) the individual G-APD detector currents are added up. This enables the detection of multiple photons over a wide dynamic range. [2]

2.2.2 Detection Efficiency

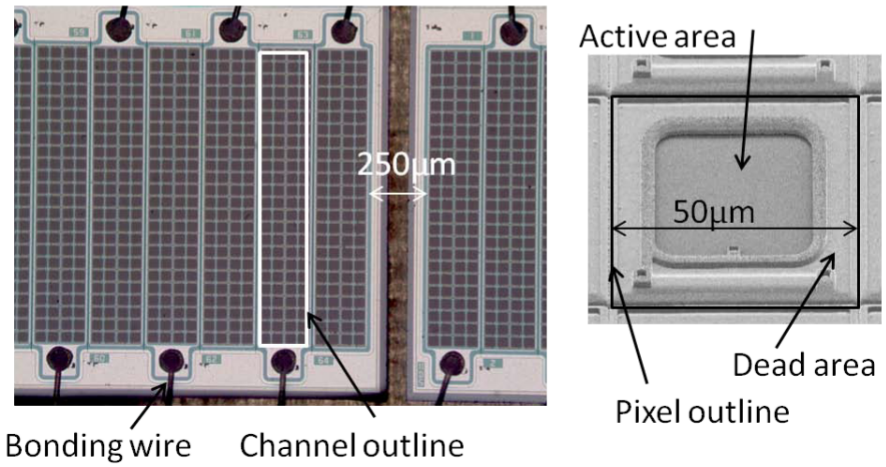

Figure 2.4 – Microscopic SiPM exposure showing the active area, dead areas and gaps. Image edited by the author. [6]

Since not all the surface of the SIPM is an active area, the detection efficiency is lowered

geometrically. The layout and areas of the SiPM can be observed in figure 2.4.

$$PDE = \frac{N_{PhEvents}}{N_{Photons}} \tag{2.3}$$

$$PDE(V) = \epsilon_{Q\lambda} \cdot P_{trig}(V) \cdot FF \qquad \lambda = const. \tag{2.4}$$

The Photo Detection Efficiency (PDE) of the SiPM determines the number of detected photons (events) versus the number of detectable photons. (equation 2.3)

The total PDE is the product of the quantum efficiency, the geometric efficiency and the Geiger efficiency, which is voltage-dependent. (equation 2.4) [7]

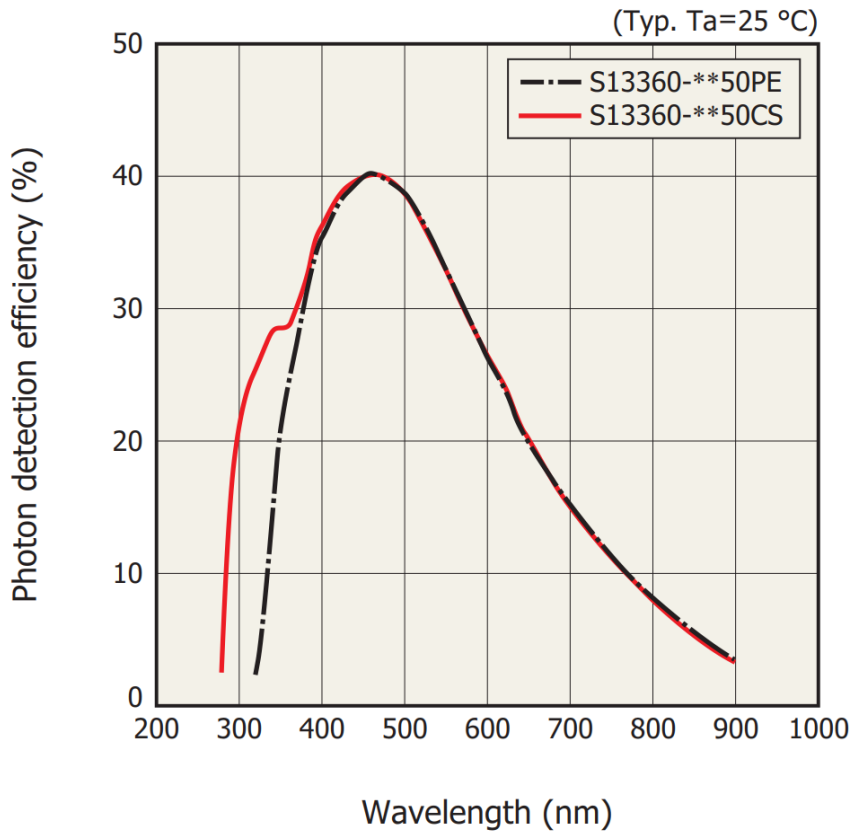

Figure 2.5 – S13360 MPPC SiPM photon detection efficiency spectral response [8]

The PDE of the used MPPC S13360-1350CS from Hamamatsu Photonics peaks conveniently at 450 nm at an efficiency of up to 50%. (see figure 2.5) This peak wavelenght matches the peak wavelenght of the scintillating fibers. [3]

2.2.3 Dark Count Events (Noise)

Because of the reverse-biased p-n junction, thermal generated electrons can also trigger an avalanche effect, without an incoming photon. This noise is referred to as a Dark Count Event, which is dependent on the overvoltage parameter. The gain and efficiency of the system profit

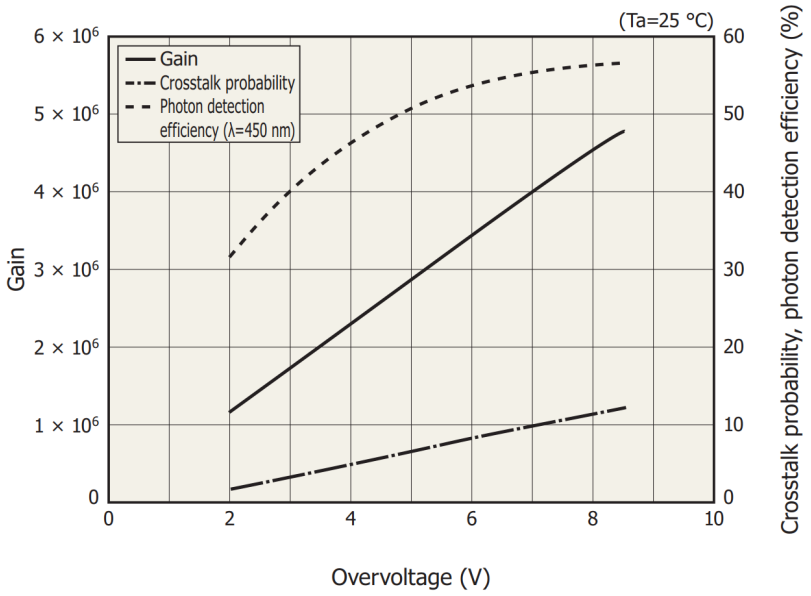

Figure 2.6 – S13360 MPPC SiPM gain, crosstalk and efficiency correlation [8]

from a high overvoltage parameter (see figure 2.6), while the Dark Count Rate also increases. [9]

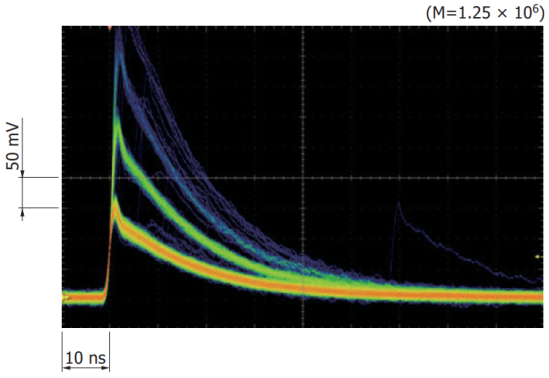

Figure 2.7 – MPPC SiPM noisy pulse waveforms [8]

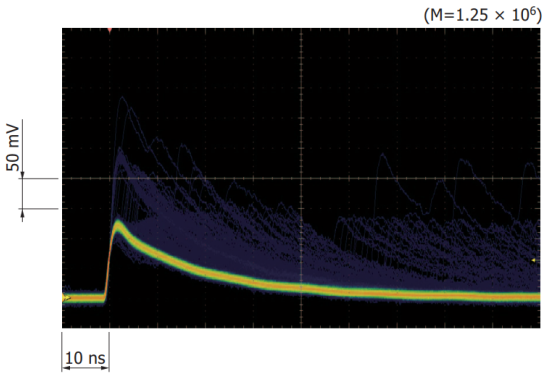

Figure 2.8 – MPPC SiPM waveforms with reducted afterpulse and crosstalk [8]

Afterpulses and crosstalk generate additional noise, as demonstrated in figure 2.8. At figure 2.7, the quantification of the output signal can be observed. Because of the parallel diodes, the resulting voltage increases with each activated diode. By setting a voltage threshold at the frontend electronics, it is possible to pre-filter the thermal noise. The higher the threshold, the

more MPPC cells have to be activated at the same time to create an event. A high threshold lowers the noise significantly, but also lowers the efficiency.

2.3 Frontend Electronics

To read out the analogue SiPM Sensors, following frontend electronics are required.

2.3.1 Requirements

The weak analogue signal coming the SiPM Sensor has to be amplified with a high SNR and digitalized into a binary signal to be readout by the FPGA.

2.3.2 Available ASICs and similar applications

The Cherenkov imaging telescope integrated read out chip (CITIROC) ASIC from Weeroc [10] is an improved version of the extended analogue silicon photo-multiplier integrated read out chip (EASIROC). [11] The EASIROC was developed for high-energy physics [12], while the CITIROC improvements were driven by astronomy requirements, including the detection of Vavilov–Cherenkov radiation in space. The CITIROC ASIC will therefore be implemented in the new Small-Sized Telescope of the Cherenkov Telescope Array (CTA) Observatory. [13]

Even though the high timing requirements for the detection of Cherenkov radiation in space don't apply in the use - case, the CITIROC ASIC is chosen for this task.

2.3.3 CITIROC ASIC relevant functions

The CITIROC ASIC features a 32 - Channel SiPM Input with adjustable gain. After pre-amplification, a Schmitt trigger outputs a binary signal on the digital output buffers. (See 2.9 "Trigger") The threshold of the Schmitt triggers can be set individually by 10-bit DAC's. For fast and easy triggering of all 32 channels, a common OR output is also provided. [11]

2.3.4 XBPF Frontend Board

The XBPF Frontend Board was developed by the CERN-BEAMS-BI group as a frontend board for scintillating fiber detectors.

The board features 192 SiPM with power supply circuits. Six CITIROC ASICs amplify and digitalize the SiPM outputs. The digital data is parallel pre-processed by a Xilinx Artix 7 FPGA and tranferred to the VFC-HD Backend Board via a SFP module with Gbit transceivers.

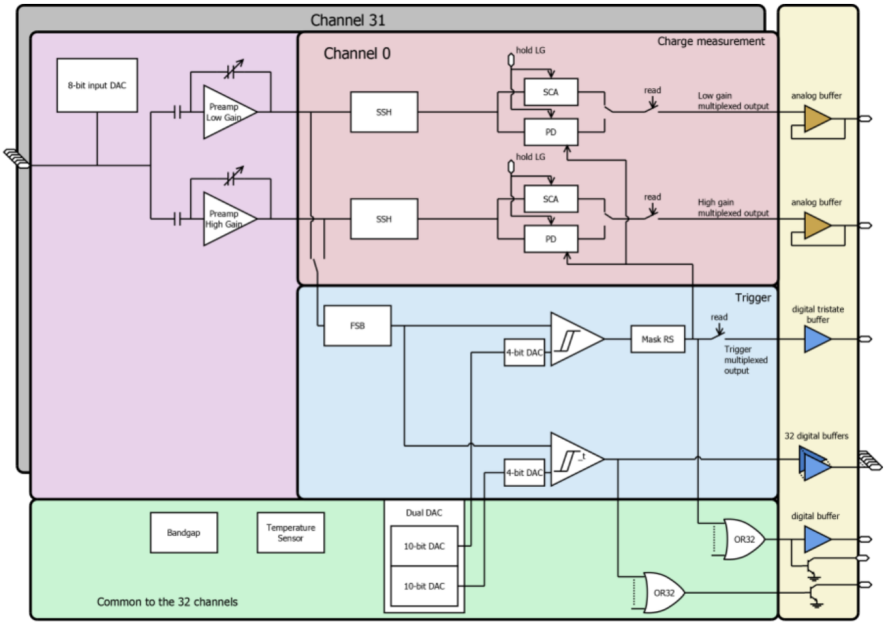

Figure 2.9 – Architecture of the CITIROC front-end ASIC [11]

2.4 Data Processing

To make the detector data available to the CERN technical network, the data has to be time-stamped and filtered by the trigger.

2.4.1 The White Rabbit Project

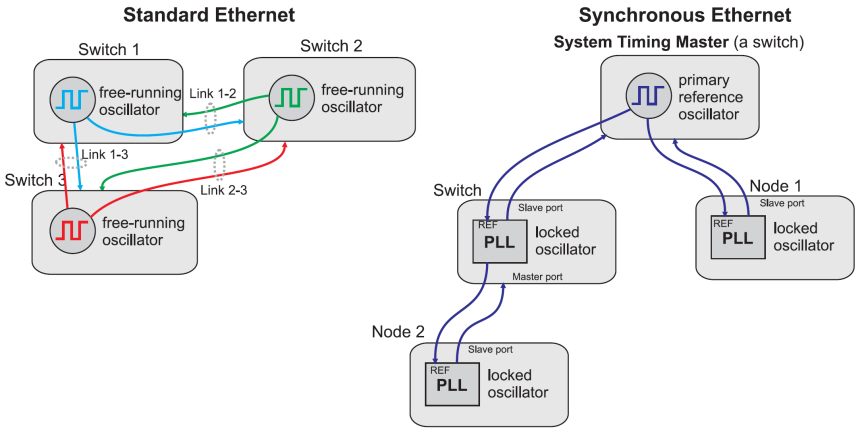

Figure 2.10 – White Rabbit Layer 1 syntonization illustration [14]

White Rabbit is an Ethernet-based sub-nanosecond synchronisation technology, initiated by CERN for accurate timing of the accelerator sites at CERN. White Rabbit measures the link delay through the exchange of time-tagged messages (PTP). In a Standard Ethernet, the nodes

encode messages by an individual, free-running oscillator, whereas Synchronous Ethernet nodes run on a oscillator that is locked to a single timing master. (Layer-1 syntonization as in Figure 2.10) To achieve better precision, the delay (phase difference) of data sent upstream by the nodes is constantly measured by a PLL and phase detector. The phase detector output allows constant monitoring and delay compensation. (Precise phase measurements) [14]

By the implementation of the three mentioned key technologies PTP, layer-1 syntonization and precise phase measurements, White Rabbit achieves sub-ns accuracy and a precision better than 50 ps over distances of the order of 10 km. [14]

The key use-case of White Rabbit relevant to the executed tasks is the precision time-tagging of measured data and triggering.
This White Rabbit system provides a clock to the VFC Backend Board with the purpose to timestamp all SiPM events.

2.4.2 VFC-HD Backend Board

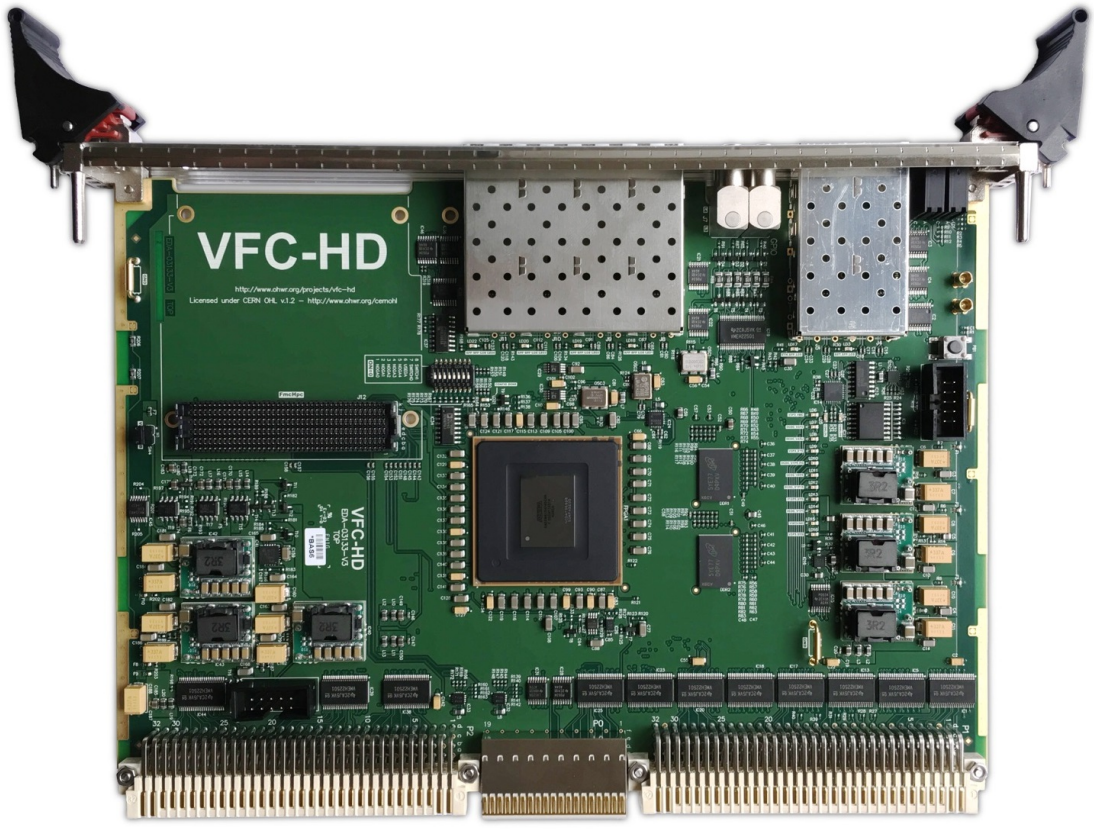

Figure 2.11 – VME FMC Carrier Board HPC-DDR3 (VFC-HD) [15]

The VFC-HD Backend Board (figure 2.11) is a VME64x board with an Altera Arria V FPGA,

developed by the Beam Instrumentation group at CERN. After decoding the stream from the optical link, the data is time-stamped by a White Rabbit signal. The timestamped trigger signals and events are saved in a ring buffer. If the timestamps are matched, the valid data is saved.

2.5 XBPF Testbench system overview

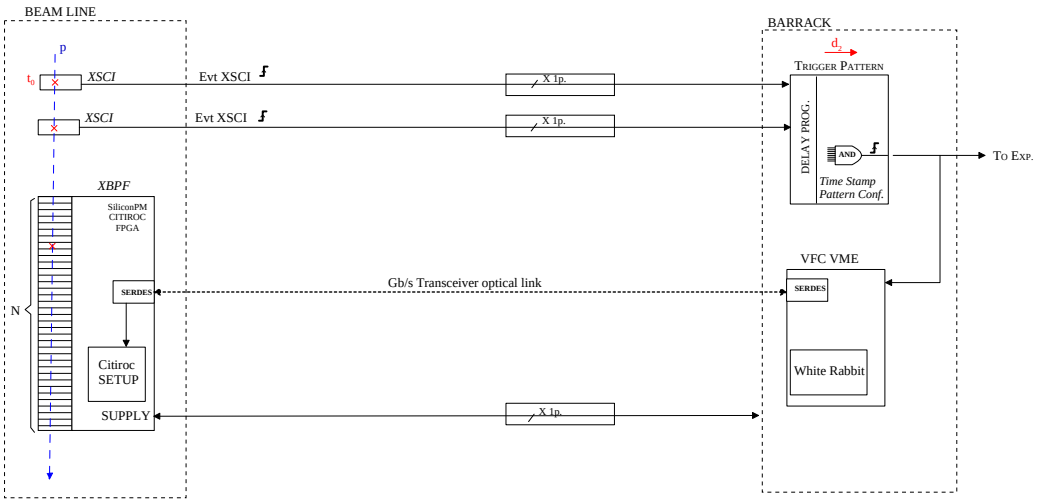

Figure 2.12 – XBPF system overview [16]

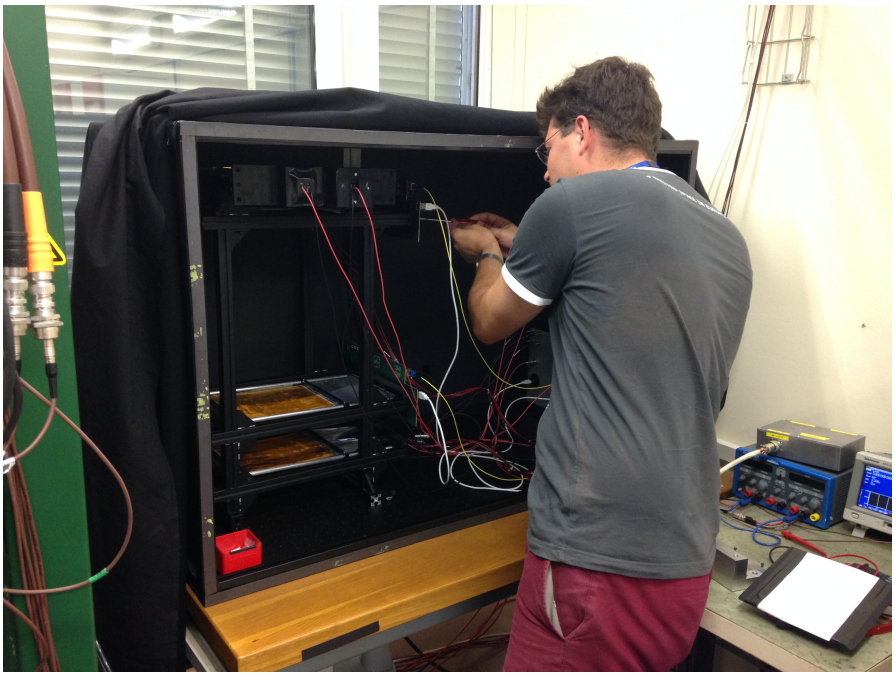

Figure 2.13 – The author installing XBPF Frontend Boards at the opened cosmic testbench. In the middle left of the testbench, the lower XBPF is visible including the orange active fiber area.

The XBPF testbench was constructed to evaluate and test the new XBPF Software and Hardware before the installation in the Neutrino Line in the CERN North Area. In the CERN North area, the XBPF Frontend Board is exposed to radiation, which makes it difficult to access and test. The Backend VFC Board however will be installed in a separate area with no or low radiation and connected to the board via rad-hard GBT optical fiber. The VME64x backplane, where the VFC Backend Boards are installed, also includes a power source for the XBPF Frontend Board. The testbench in the laboratory simulates the same setup: The VME Backend is in a separate room, supplying power and connecting to the XBPF Frontend Board by GBT optical fiber. Details are provided in figure 2.12

Figure 4.9 shows the VFC Backend in VME64x crate in the separated lab room during signal measurements.

2.5.1 Geometry

In the laboratory, the Frontend Subsystem is installed in a physical black box, designed to isolate the systems from ambient light. (See figure 2.14) The system is pointed upwards to the sky with the purpose to calibrate the XBPF with high energy muons, created in the upper atmosphere by cosmic rays. On the lower and upper end of the detector, two new scintillating fiber triggers are installed. They are shifted 90 degrees to create a square active area of 192mm

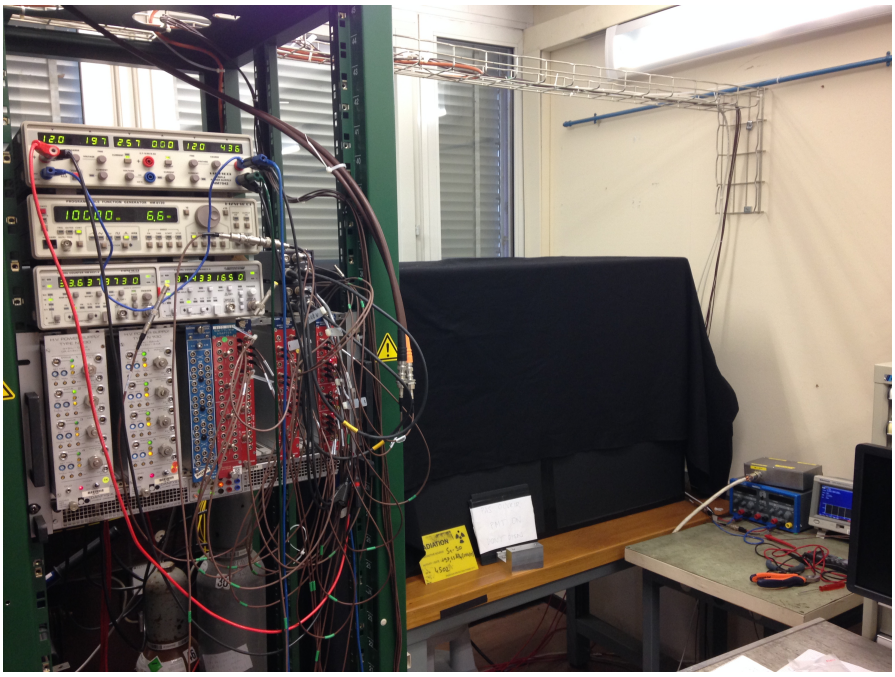

Figure 2.14 – The covered testbench while exposed to a Strontium^{90} beta source. (197 KBq, 0.546 MeV) Front left: Counters indicating 33 and 37 events per second

X 192mm. In between the triggers, there are two XBPF frontend detectors installed with the fibers in parallel in the active area. This setup only creates a one-dimensional dataset, but allows better system verification. (compare to figure 2.13)

2.5.2 External Trigger

The two triggers of the testbench, mentioned in Section 2.5.1, ensure that a high energy particle, that crosses the two triggers, also crosses the two frontend XBPF detectors. This is possible by logically connecting the output signal of the triggers with an AND Gate.

$$\Delta t_{Trigger} = \frac{x_{Trigger2-Trigger1}}{0.99c} = \frac{0.615m}{296794533m/s} = 2.07ns \tag{2.5}$$

Because atmospheric muons have an energy of at least 2 GeV, their velocity is close to the speed of light. They cross the trigger planes, that are 61.5 cm apart, in 2.07 nanoseconds. (equation 2.5)

This time offset $\Delta t_{Trigger}$ is much smaller than the flag width of the CITIROC trigger signal (100-500 ns), which allows the simplification, that the particle crosses all planes "at the same time". With this coincidence triggering setup, it is made sure that the particle crosses all four planes and is not a noise / dark count event (DCE). This AND coincidence signal is further referred to as "External Trigger".

3 XBPF System Improvements

In this chapter, the improvements of the detector systems are discussed. For each improvement the problem and the solution is described and verified in a uniform way. The improvements are implemented in the generation of XBPF detectors that is being installed in the CERN North Area from August 2018. The hardware updates of Xilinx and Intel FPGAs was implemented in orientation on the V-Model XT development cycle and the use of version control.

3.1 Channel Masking

This section explains the solution of masking chosen channels of a XBPF Detector. The system requirements are validated and the FPGA update is verified by measurement.

3.1.1 Problem

As discussed in section 2.2.3, noise (DCE) is a central problem for the XBPF operation. By using the external trigger coincidence, (section 2.5.2) most noise can be suppressed. However, individual SiPM units can break and cause more noise, or even a constant active signal. Those channels would indicate a particle at every trigger, which is maskable by software at the data analysis level.

Although this can be a problem because of larger generated data, the main problem appears by using the output of the SiPMs for triggering the system, like described in the sections 3.2 and 3.3. In this case, the faulty channels would cause constant triggering, which prevents the coincidence from suppressing noise and could cause trigger overflows.

This is the motivation for the development of a Channel Masking System for the XBPF.

3.1.2 Requirements

Following requirements were defined for the Channel Masking System:

- Each channel must be maskable individually.
- More than one channel must be maskable.
- The mask should be defined in a memory register on the VFC.
- The mask should be implemented on hardware levels.
- The mask should be implemented in the frontend board.
- The mask must be applied before the cross/self trigger.
- The mask should be applied before the optical link interface.
- The new registers should not be implemented in the same address space as the control registers.

3.1.3 Solution

The basic idea to achieve channel masking is the creation of a register, which is then connected by a logic AND to a data acquisition vector to mask the chosen channels. Also, the register in the VFC Backend has to be assigned to the XBPF Frontend register.

Frontend FPGA update

```
1  always \@*
2    casez(Adr_ib21)
3      21'b0_0000_0000_0000_0000_????: SelectedModule_b8 =
         c_SelCtrlReg; // FROM 00_0000 TO 00_000F (WB)
4      //== FROM 00_0000 TO 00_003C (VME) <-   16 regs ( 16B)
5      21'b0_0000_0000_0000_001?_????: SelectedModule_b8 =
         c_SelStatReg; // FROM 00_0020 TO 00_003F (WB)
6     // == FROM 00_0080 TO 00_00FC (VME) <-   32 regs ( 16B)
7      21'b0_0000_0000_0000_0100_????: SelectedModule_b8 =
         c_SelMaskReg; // FROM 00_0080 TO 00_008F (WB)
8      //== FROM 00_0100 TO 00_013C (VME) <-   16 regs ( 16B)
9      default:                          SelectedModule_b8 =
         c_SelNothing;
10   endcase
```

Listing 3.1 – Mask Register Address Decoding in xbpf_AddrDecoderWbApp.v

To create a memory space for the mask, the address decoding function in xbpf_AddrDecoderWbApp.v were modified. The address space is created and selected with adding a case to the Address Decoder. (listing 3.1) The five registers "xbpf_reg_mask_X_b32" are assigned to this space.

```
signal xbpf_WbDatMaskReg_b32 : std_logic_vector(31 downto 0);
signal xbpf_WbAckMaskReg : std_logic;
signal xbpf_WbStbMaskReg : std_logic;

signal xbpf_reg_mask_0_b32  : std_logic_vector(31 downto 0);
signal xbpf_reg_mask_1_b32  : std_logic_vector(31 downto 0);
signal xbpf_reg_mask_2_b32  : std_logic_vector(31 downto 0);
signal xbpf_reg_mask_3_b32  : std_logic_vector(31 downto 0);
signal xbpf_reg_mask_4_b32  : std_logic_vector(31 downto 0);
signal xbpf_reg_mask_5_b32  : std_logic_vector(31 downto 0);
  [...]
   real_event_mask_b192 (191 downto 160) <=  xbpf_reg_mask_5_b32;
   real_event_mask_b192 (159 downto 128) <=  xbpf_reg_mask_4_b32;
   real_event_mask_b192 (127 downto 96)  <=  xbpf_reg_mask_3_b32;
   real_event_mask_b192 (95 downto 64)   <=  xbpf_reg_mask_2_b32;
   real_event_mask_b192 (63 downto 32)   <=  xbpf_reg_mask_1_b32;
   real_event_mask_b192 (31 downto 0)    <=  xbpf_reg_mask_0_b32;
```

Listing 3.2 – Transfer of 5 mask registers to 192 bit event mask in xbpf_detector_top.vhd

These five mask registers from the Wishbone Bus (VFC) are assigned to a single mask vector with 192 bits in xbpf_detector_top.vhd. (Listing 3.2) Each bit represents one masked SiPM, which connects to a fiber.

```
signal masked_event_data_b192 : std_logic_vector(191 downto 0);
[...]
masked_event_data_b192    <= sCITIROC_SiPm AND
  real_event_mask_b192;
[...]
    process (clk_event_10m, reset_rn ) is
    begin
        if reset_rn = '0' then
            event_valid_q <= '0';
            event_valid_ctr_qb4 <= x"0";
            event_data_qb192 <= (others => '0');
        else rising_edge( clk_event_10m ) then
                [...]
                event_valid_q       <=  '1';
                event_data_qb192    <= masked_event_data_b192;  --
                   Masked sCITIROC_SiPm with channel mask register
                [...]
        end if;
    end process;
```

Listing 3.3 – Masking CITIROC signal in xbpf_detector_top.vhd

Finally, the vector from the CITIROC IC's is masked with a logical AND connection. The masked event data is then sampled at 10 MHz on the rising edge in a process. (Listing 3.3)

VFC Control registers

From the VFC Backend, the control registers in table 3.1 are forwarded to each XBPF device separately: [17]

Register	r/w	Address	Depth	Basic info	In UI
D0DEVMASK0	rw	0X850100	1	Data bit mask LSB	yes
	Masks 32 LSB of the 192bit vector: Ch 31 - 0				
D0DEVMASK1	rw	0X850104	1	Data bit mask	yes
	Masks second 32 bits of the 192bit vector: Ch 63 - 32				
D0DEVMASK2	rw	0X850108	1	Data bit mask	yes
	Masks third 32 bits of the 192bit vector: Ch 95 - 64				
D0DEVMASK3	rw	0X85010C	1	Data bit mask	yes
	Masks fourth 32 bits of the 192bit vector: Ch 127 - 96				
D0DEVMASK4	rw	0X850110	1	Data bit mask	yes
	Masks fifth 32 bits of the 192bit vector: Ch 159 -128				
D0DEVMASK5	rw	0X850114	1	Data bit mask MSB	yes
	Masks 32 MSB of the 192bit vector: Ch 191 -160				

Table 3.1 – Device 0 Channel Masking Registers of the VFC [17]

3.1.4 Validation

All "must" and "should" requirements of section 3.1.2 are met with the improved system. Since the masking AND was implemented after the I/O processing of the CITIROC output on the XBPF Frontend, no triggers are generated as the data is not sent over the optical link.

3.1.5 Verification

Register	Value	Reason
D0DEVMASK0	0xFFFFFFFF	No masking of channels 31 - 0
D0DEVMASK1	0xFFFFFFFF	No masking of channels 63 - 32
D0DEVMASK2	0xFFFFFFFF	No masking of channels 95 - 64
D0DEVMASK3	0xFFFFFFFF	No masking of channels 127 - 96
D0DEVMASK4	0xFFFFFFFF	No masking of channels 159 -128
D0DEVMASK5	0xDFDFFFFF	Masking noisy channels 181 and 189 by deleting bits 21 and 29

Table 3.2 – Register configuration for masking noisy channels 181 and 189 on device 0

To verify the channel masking function, the two most noisy (DCR) channels of device 0 were masked using the register configuration in table 3.2.

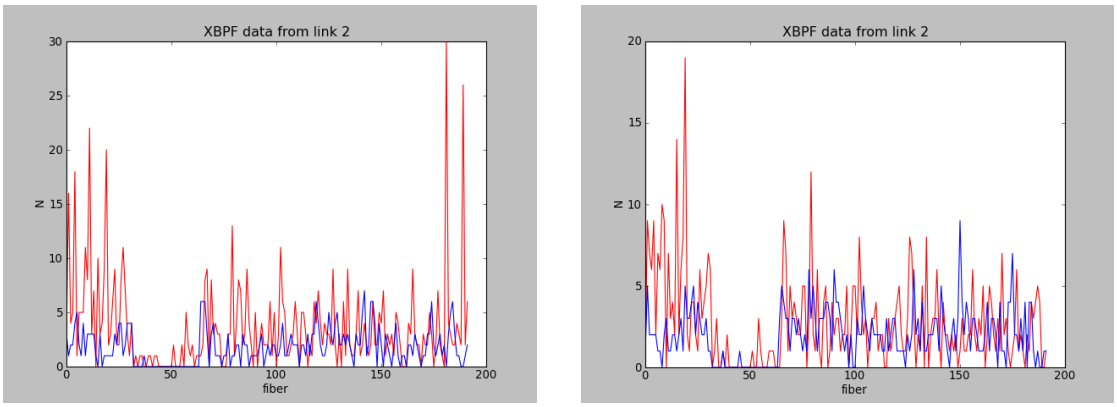

(a) Unmasked profile

(b) Same profile, masked channels 181,189

Figure 3.1 – Mask comparison of Self Trigger XBPF Frontend acquisition data of device 0 and 1 at threshold 260. Events per fiber in 10 seconds

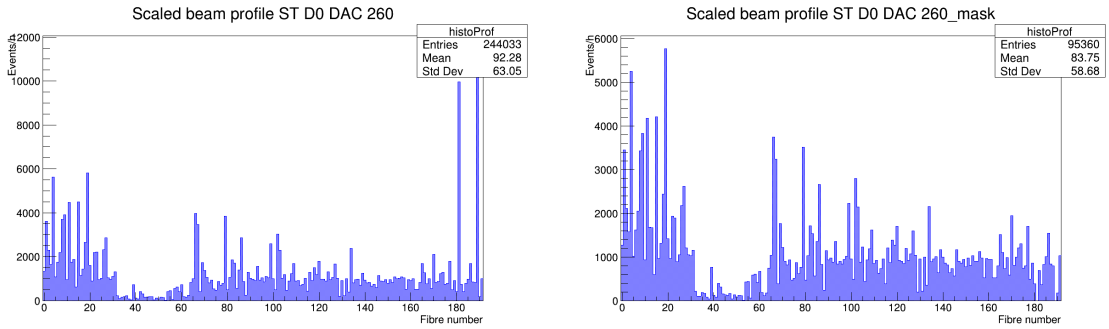

(a) Unmasked profile

(b) Masked channels 181 and 189 profile

Figure 3.2 – Mask comparison of analysed Self Trigger datasets of device 0 at threshold 260.

The self - trigger measurements in the figures 3.1a and 3.2b show the generated dark count events of device 0. The channels 181 and 189 are generating noise with a DCR of 11000 events per hour. After the application of the mask, channels 181 and 189 read zero events in live frontend acquisition mode (figure 3.1b) and in the finished profile (figure 3.2b).

3.2 Acquisition without coincidence triggering (Self Triggering)

This section explains the system improvement to enable the triggering of individual planes without an external trigger.

3.2.1 Problem

In the beamline commissioning phase, the complex system of magnets, scintillators (triggers) and the XBPF must be adjusted to create a stable beamline. In this state, no external trigger is provided to the XBPF systems. (see section 5.2) Therefore, the system has to be able to trigger itself to create an estimated beam profile.

This acquisition mode is also useful to make a profile of the DCE without any beam. This leads to a better understanding of the noise in the system.

At high activity beams, this mode is also useful, because the activity of the beam is much higher than the DCR. For activity estimation, the noise is not relevant compared to the high activity beam.

3.2.2 Requirements

- The system must acquire data without an external trigger.
- The system must acquire data with or without a second XBPF Frontend.
- The system must acquire raw data for testing.
- The system should use the same multiplexing functions as the L3 and L4 connector outputs.
- The new registers should be implemented in the same address space as the control registers.

3.2.3 Solution

For the self - trigger mode the FPGA of the VFC Backend was updated. New registers were introduced which are accessible by a FESA class to allow remote mode configuration. To also accommodate the cross trigger mode (section 3.3) and stay consistent with the previous functionality, the multiplexer `module activity_flag` was used for mode selection.

Mode system overview

Instead of relying on the AND coincidence of the two external triggers, it is sufficient for the self trigger to use their trigger/activity `output activity_o` as its `input SeTtrig_i`. No further logical processing is required. (See figure 3.3) The external triggers are not needed, but remain in the testbench for system verification and testing.

Backend FPGA update

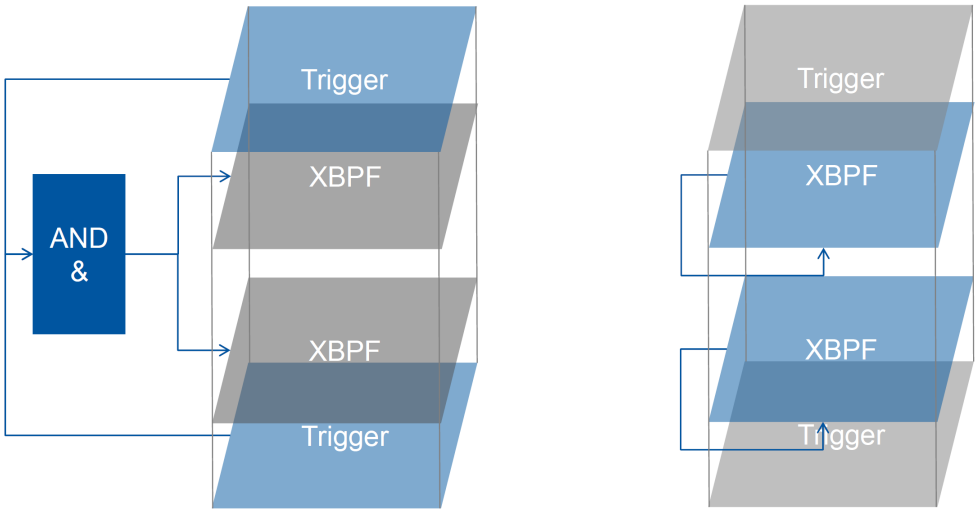

(a) External Trigger (b) Self Trigger

Figure 3.3 – Comparison charts of Self Trigger mode with External Trigger. The trigger sources are represented by the color light blue

```
wire Dev0Activity;
wire Dev0SeTrig;

i_xbpf_device_0 (
    .sys_clk_ik( a_Clk_k ), // System 125 MHz clock
    .reset_ir( reset_r ),   // Asynchronous reset
    [...]
    .SeTtrig_i(Dev0SeTrig), // Self / Cross Trigger
    .activity_o( Dev0Activity ) // Device Activity Indicator
);
```

Listing 3.4 – Frontend device 0 variable declaration and Self/Cross Trigger instantiation in VfcHdApplication.sv

In the top-file VfcHdApplication.sv, the new `wire DevXSeTrig` and `wire DevXActivity` are defined for every device in System Verilog. (see listing 3.4)

```
module xbpf_device_top(

    input sys_clk_ik, // System 125 MHz clock
    input reset_ir,   // Asynchronous reset
    [...]
    input SeTtrig_i,
    output activity_o,   // activity flag
);
```

Listing 3.5 – Input and Output declaration of xbpf_device_top module in xbpf_device_top.v

These wires (VHDL: "signals") are connected to the `input SeTtrig_i` and the `outout activity_o` (see figure 3.5) of the instantiation of each corresponding `module xbpf_device_top`. (see figure 3.6)

```
activity_flag SeT_activity_flag(

    .sys_clk_ik( a_Clk_k ), // System 125 MHz clock
    .reset_ir( reset_r ),   // Asynchronous reset

    // input
    .Dev0Activity_i( Dev0Activity ), // Activity Flag from Device 0
    .Dev1Activity_i( Dev1Activity ), // Activity Flag from Device 1

    // configuration registers
    .FlagL3Src_ib3(FlagSeT0Src_b3),
    .FlagL4Src_ib3(FlagSeT1Src_b3 ),
    .FlagL3Width_ib32(FlagSeT0Width_b32),
    .FlagL4Width_ib32(FlagSeT1Width_b32),

    // Trigger output
    .L3Gpio_oq(Dev0SeTrig ),
    .L4Gpio_oq(Dev1SeTrig )
);
```

Listing 3.6 – Multiplexer Module instantiation for Self/Cross Trigger generation in VfcHdApplication.sv

This module also needs the White Rabbit clock, an asynchronous reset, and the configuration registers as inputs for the instantiation. The function of the multiplexers and the configuration registers are documented in section 3.2.3.

```
assign trigger = (L1_i & trigger_select_b5[0] ) |
             (L2_i & trigger_select_b5[1] ) |
             (trigger_sw & trigger_select_b5[2] ) |
             (trigger_periodic_qb4[3] & trigger_select_b5[3])|
             (SeTtrig_i & trigger_select_b5[4] );
             // self/cross trigger
```

Listing 3.7 – Trigger Mode Assignment in xbpf_device_top.v

To assign the multiplexed `wire SeTtrig_i` Self Trigger input to the active trigger function, bit 4 of the register D0TRGSEL is added and multiplexed to the input. For reference see the listing 3.7 and the register table 3.3.

VFC Control registers

Register	r/w	Address	Depth	Basic info	In UI
D0TRGSEL	rw	0x840008	1	Trigger source selector.	yes
Selects trigger source for the device. Bits: 0 L1 input 1 L2 input 2 software trigger (D0TRGSW) 3 periodic internal trigger 4 internal self/cross trigger (D0STFLAGSRC)					
D0STFLAGSRC	rw	0x800018	1	D0 self trigger flag source	no
Configures source for device 0 self/cross trigger activity flag (OR of 192 bits) and its combination. Keep combination at OR with one active source. Bits: 0 activate device 0 1 activate device 1 2 OR (0) AND (1)					
D0STFLAGWIDTH	rw	0x80001C	1	D0 self trigger flag width	no
Configures the time the flag remains high after triggered by event. In 125 MHz White Rabbit clock ticks. All 32 bits available.					

Table 3.3 – Device 0 Trigger Registers of the VFC [17]

The registers in the VFC Backend in table 3.3 were created or modified to allow the self trigger configuration. The register DXTRGSEL is connected to the `reg trigger_select_b5`, register DXSTFLAGSRC to `reg FlagSeTXSrc_b3` and DXSTFLAGWIDTH to `reg FlagSeTXWidth_b32`.

```
[cfv-865-bitb]  /user/mraudoni/xbpf  > source set_vfc_st.sh

XBPF-VFC ST Trigger register initialisation

DEVICE0 = XBPF0

D0 Trigger source was set to ST/CT (0x10) ... OK
D1 Trigger source was set to ST/CT (0x10) ... OK
D0 Trigger offset was set to 0 8ns-WR-clock-ticks ... OK
D1 Trigger offset was set to 0 8ns-WR-clock-ticks ... OK
D0 S Trigger source was set to D0 (0x1) ... OK
D1 S Trigger source was set to D1 (0x2) ... OK
D0 Self Trigger Flagwidth was set to: 0x0000000f (15 8ns-WR-clock-ticks)
 -> Setting Self Trigger Flagwidth to 15 8ns-WR-clock-ticks ... OK
D1 Self Trigger Flagwidth was set to: 0x0000000f (15 8ns-WR-clock-ticks)
 -> Setting Self Trigger Flagwidth to 15 8ns-WR-clock-ticks ... OK
```

Figure 3.4 – Script setting both devices into Self-Trigger Mode

To facilitate changing of the trigger modes, the script set_vfc_st.sh was created that reads, interprets and sets the correct register values, listed in table 3.4. An example script output is

shown in figure 3.4.

3.2.4 Validation

All "must" and "should" requirements of section 3.2.2 are met with the improved system. By reusing the multiplexer module for the L3 and L4 outputs, the system is less susceptible to errors and the register functions are consistent.

3.2.5 Verification

Register	Value	Reason
D0TRGSEL	0x10	Trigger source: internal self/cross trigger
D0STFLAGSRC	0x1	Trigger from Device 0
D0STFLAGWIDTH	0xF	Must be greater than 12.5 due to sampling a 10 MHz flag with 125MHz
D1TRGSEL	0x10	Trigger source: internal self/cross trigger
D1STFLAGSRC	0x2	Trigger from Device 1
D1STFLAGWIDTH	0xF	Must be greater than 12.5 due to sampling a 10 MHz flag with 125MHz

Table 3.4 – Device 0 and 1 Register Values in Self-Trigger Mode

To set a XBPF device in Self Trigger mode, the registers DXTRGSEL, DXSTFLAGSRC and DXSTFLAGWIDTH were set to 0x10, 0x1/0x2 and 0xF. (See register table 3.4)

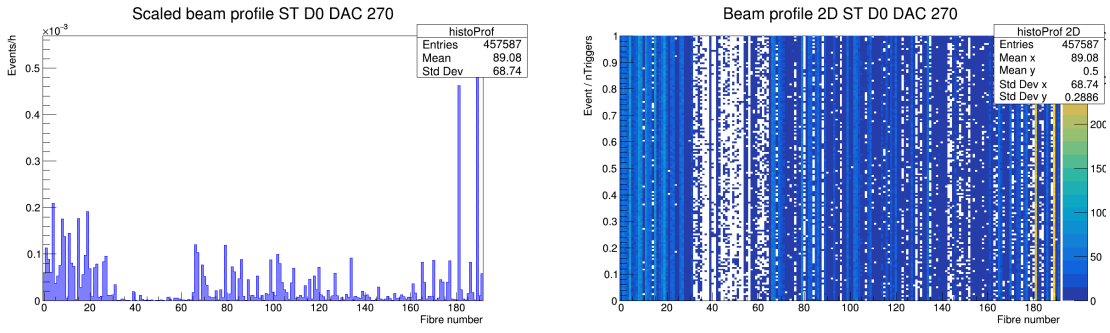

(a) Self Trigger (ST) Profile

(b) ST Profile over the number of events

Figure 3.5 – Device 0 Self Trigger profiles, threshold 270

The resulting DCR (noise) profiles were equal to the manual XBPF Frontend readout profiles. Figure 3.5 shows the resulting profile at threshold 270. In figure 3.5b, the DCR is plotted against the number of events. This allows the successful verification of the consistency and macroscopic stability of this trigger mode: At the same temperature and threshold, every SiPM has a different stable DCR.

3.3 Coincidence triggering using two monitors (Cross Triggering)

3.3.1 Problem

To cancel the SiPM noise (DCE), two or more trigger planes have to be connected with an AND coincidence.

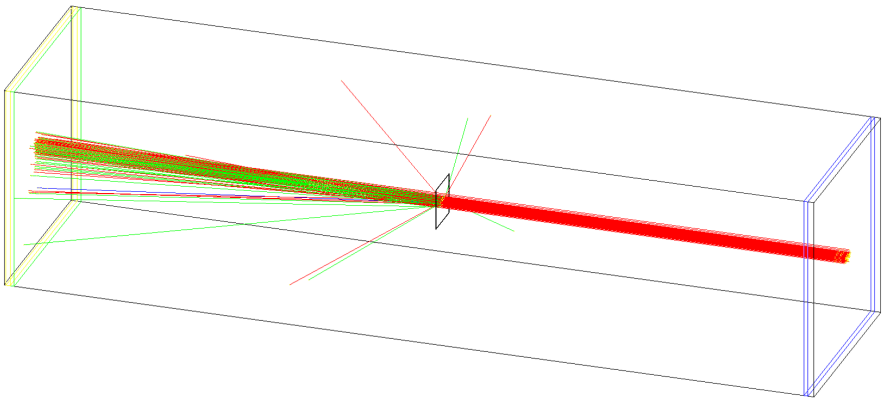

(a) 3D Simulation

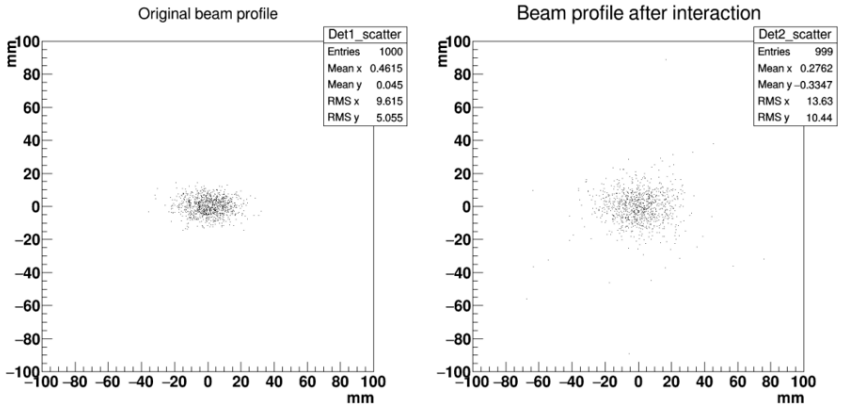

(b) Profile 1 meter before and behind interaction fibers

Figure 3.6 – Simulation of beam interactions with a fiber plane. The beam is composed of 1000 electrons of 1 GeV/c. [16]

The simulations 3.6a and 3.6b show the interaction of particles with the fiber plane. Ideally, a beam monitor measurement system should not interfere with the beam. Because of the fiber planes in the way of the beamline, this can not be prevented. However, the number of fiber planes can be reduced by the removal of the trigger planes and the creation of the AND coincidence with the XBPF Frontend Boards. This also decreases the system cost and complexity.

3.3.2 Requirements

- The system must acquire data without an external trigger.
- The system must acquire data with a second XBPF Frontend.
- The system must significantly cancel DCE noise.
- The system must acquire data from both frontend devices.
- The system should be able to additionally output the trigger signal at the L3 and L4 connector outputs.
- The system should use the same multiplexing functions as the L3 and L4 connector outputs.
- The new registers should be implemented in the same address space as the control registers.

3.3.3 Solution

By updating the VFC Backend FPGA, the `wire DevXActivity_i` connects over a `module activity_flag` multiplexer to the trigger output `wire DevXSeTrig`. This is described in section 3.2.3. The multiplexer can also be configured to an AND coincidence between both devices. This mode is to be further addressed to as Cross Trigger Mode.

Mode system overview

Instead of relying on the External Triggers for noise cancellation (figure 3.7a), the Cross Trigger Mode creates the coincidence with the two XBPF Frontends and (cross-) triggers the system (figure 3.7b). The external triggers are not needed, but remain in the testbench for system verification and testing.

VFC Control registers

Like the Self Trigger Mode, the VFC Backend can be configured using the registers DXTRGSEL, DXSTFLAGSRC and DXSTFLAGWIDTH. (compare to section 3.2.3)

To change the trigger modes automatically, the script set_vfc_ct.sh was created that reads, interprets and sets the correct register values, listed in table 3.5. An example script output is shown in figure 3.8.

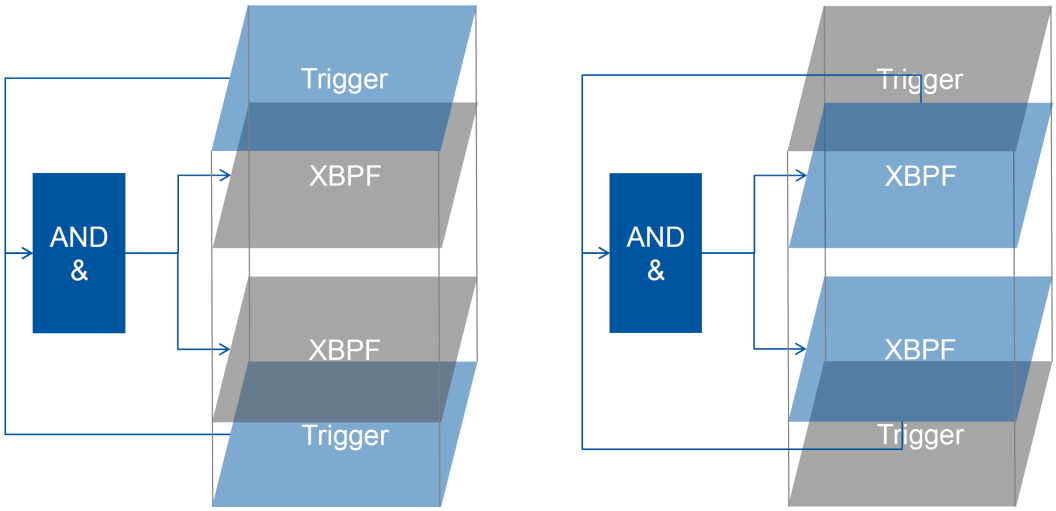

(a) External Trigger (b) Cross Trigger

Figure 3.7 – Comparison charts of Cross Trigger mode with External Trigger. The trigger sources are represented by the color light blue

```
[cfv-865-bitb]  /user/mraudoni/xbpf  > source set_vfc_ct.sh

XBPF-VFC CT register initialisation

DEVICE0 = XBPF0

D0 Trigger source was set to ST/CT (0x10) ... OK
D1 Trigger source was set to ST/CT (0x10) ... OK
D0 Trigger offset was set to 0 8ns-WR-clock-ticks ... OK
D1 Trigger offset was set to 0 8ns-WR-clock-ticks ... OK
D0 S Trigger source was set to: 0x00000001
 -> Setting S D0 Trigger source to CT  (0x7) ... OK
D1 S Trigger source was set to: 0x00000002
 -> Setting D1 S trigger source to D1 (0x7) (testbench default)... OK
D0 Self Trigger Flagwidth was set to: 0x0000000f (15 8ns-WR-clock-ticks)
 -> Setting Self Trigger Flagwidth to 15 8ns-WR-clock-ticks ... OK
D1 Self Trigger Flagwidth was set to: 0x0000000f (15 8ns-WR-clock-ticks)
 -> Setting Self Trigger Flagwidth to 15 8ns-WR-clock-ticks ... OK
[cfv-865-bitb]  /user/mraudoni/xbpf  >
```

Figure 3.8 – Script setting both devices into Cross-Trigger Mode

3.3.4 Validation

All "must" and "should" requirements of section 3.3.2 are met with the improved system. By reusing the multiplexer module for the L3 and L4 outputs, the system is less susceptible to errors and the register functions are consistent. This also allows to output the trigger signal at the L3 and L4 outputs in the same way.

3.3.5 Verification

To set the XBPF device in Cross Trigger mode, the registers DXTRGSEL, DXSTFLAGSRC and DXSTFLAGWIDTH were set to 0x10, 0x7 and 0xF. (See register table 3.5)

Register	Value	Reason
D0TRGSEL	0x10	Trigger source: internal self/cross trigger
D0STFLAGSRC	0x7	Trigger from device 0 AND 1
D0STFLAGWIDTH	0xF	Must be greater than 12.5 due to sampling a 10 MHz flag with 125MHz
D1TRGSEL	0x10	Trigger source: internal self/cross trigger
D1STFLAGSRC	0x7	Trigger from device 0 AND 1
D1STFLAGWIDTH	0xF	Must be greater than 12.5 due to sampling a 10 MHz flag with 125MHz

Table 3.5 – Device 0 and 1 Register Values in Cross-Trigger Mode

Verification with Strontium-90 radiation sources

The first functional tests of the Cross Trigger were conducted using two Strontium^{90} sources with decay rates of 197 KBq and 21Mbq. Strontium^{90} almost exclusively β^- decays into electrons with 0.546 MeV. The advantage of the verification with Strontium^{90} is the event rate of up to 21 million particles per second. This way, conclusive test beam profiles can be created within minutes.

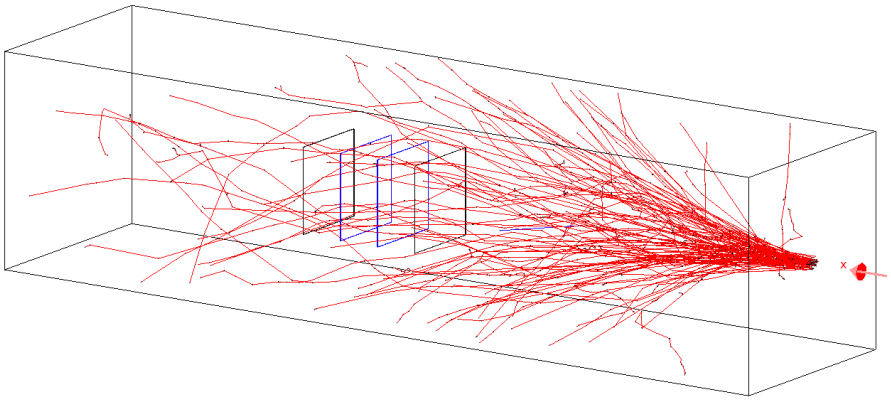

Figure 3.9 – XBPF Test Bench Simulation of a 1 MeV electron beam with Geant4. Credit: Dr. Inaki Ortega. Modified by the author.

The problem of this measurement method is the interaction of the low-energy particles with the atmospheric air and the fiber planes. As simulated in figure 3.9, the electrons strongly interact with the atmosphere and the majority of the particles does not cross all four fiber planes of the measurement setup. Individual particles cross the upper trigger plane (figure 3.9 black plane on the right), go around the XBPF Trigger planes (blue) and hit the lower fiber plane (figure 3.9 black plane on the left). This would suggest a valid event, which is not registered at the XBPFs because of system malfunction or inefficiency.

Therefore, for further verification and analysis, this method is insufficient. All following measurement profiles are created using cosmic muons, unless otherwise stated.

Verification with cosmic muons

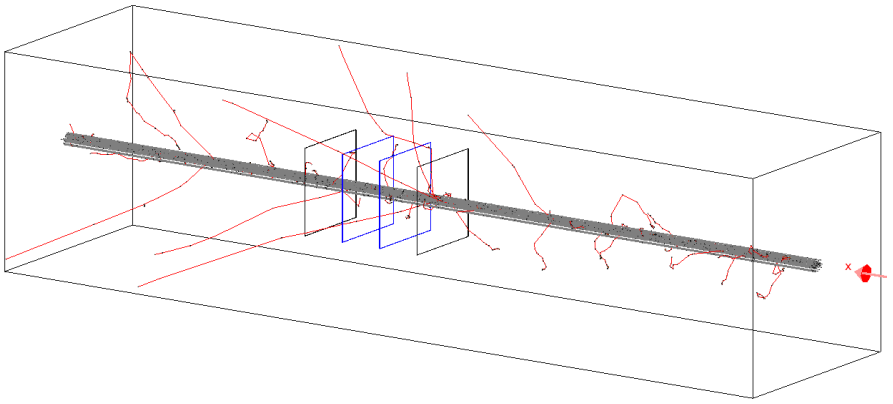

Figure 3.10 – XBPF Test Bench Simulation of a 10 GeV muon beam with Geant4. Credit: Dr. Inaki Ortega. Modified by the author.

Cosmic muons have an energy greater than 2 GeV and show much less deviation and interaction with atmospheric particles. All trigger planes are crossed by the particles and only secondary particles (red) could trigger a multiplicity event. (figure 3.10) This measurement method is more suitable for the XBPF system performance and efficiency analysis, further elaborated in chapter 4.

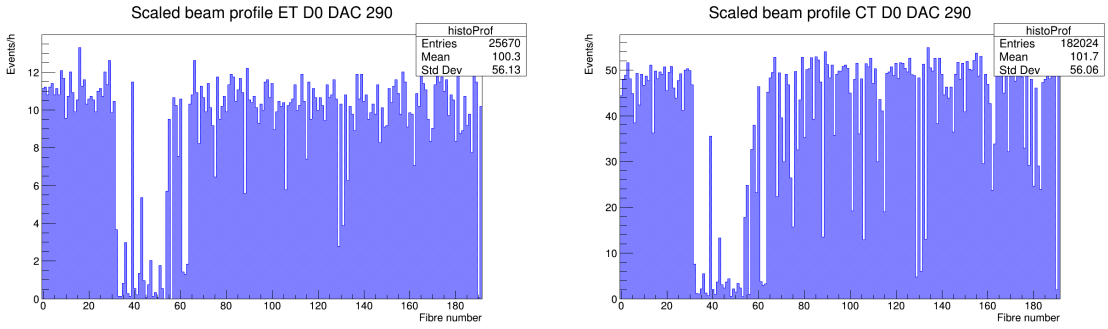

(a) External Trigger

(b) Cross Trigger

Figure 3.11 – Comparison of External and Cross Trigger Profiles at device 0, threshold 290

Figure 3.11 verifies the function of the Cross Trigger. The External Trigger registered 25670 fiber hits in 1034 Minutes. The Cross Trigger registered 182024 fiber hits in 1472 minutes at the threshold 290. Because of the long exposure to cosmic radiation, the profiles match visually. This confirms the functionality of the Cross Trigger. The big difference between the two plots is the rate of events: While the External Trigger detects 25,92 events per minute, the Cross Trigger detects 97.50 events per minute. This a 3.76 fold increase in detected events can be explained due to the different efficiency combinations of each mode. This is further discussed in section 4.4.5.

The system successfully cancels noise (DCE), but like with external triggers, there is still a small chance of two DCE happening at the same time, especially at low threshold levels.

In Chapter 4 many conclusive measurements were conducted and analysed to further comprehend the behaviour of the system.

3.4 Integration

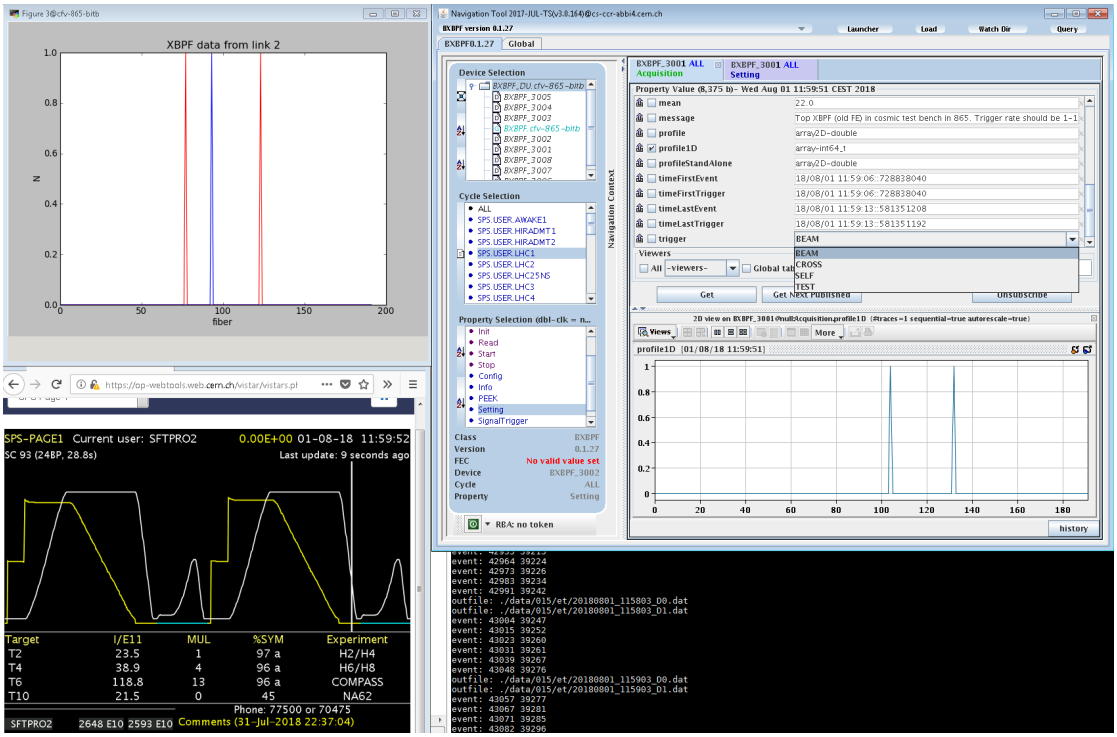

Figure 3.12 – Parallel data acquisation by a script and the SPS cycle-synchronised FESA Class in the CERN technical network

By using FESA Classes, all authorized researchers at CERN and the corresponding institutes can access the data of the XBPF System. For later application, the data is synchronized to SPS extractions. Through a drop-down menu, the desired trigger mode can be chosen over the technical network. (see figure 3.12)

4 Data Analysis

The second result-focused part of this thesis is the analysis of measurement data to further test the system and develop new analysis software, which can be used in future applications.

4.1 Acquired Dataset

First, the data had to be acquired using the script xbpf_data_acquire.py. Fifteen standard protocol measurements were conducted, with each of the three ET, ST, CT modes planned. One measurement typically takes 3 days, because to collect enought data with cosmic mouns, the measurement should run 24h for the modes ET and CT. Measurements 001-003 were flawed because of an incorrect setting of DXFLAGWIDTH. This led to the exclusion of these measurements. Measurements 004-007 were conducted without any apparent problem. Measurements 008-015 are flawed, because on device 1, the second CITIROC ASIC malfunctioned, which led to a decreased detection rate on fibers 32-64. To use these measurements for efficiency and noise considerations like intended, the fibers 32-64 were excluded in an altered analysis program, to allow comparisons with measurements 001-003. For efficiency calculations, these channels were masked and the number of hits compensated by multiplication with $\frac{6}{5}$. In addition, extra measurements, like the moving source test were made. The efficiency calculations in section 4.8 show that there was an error with the experimental testbench setup. Therefore, these results are limited to this setup.
The measurement log is pasted in the appendix listing A.1.

4.2 Data Analysis framework

Because the existing measurement and analysis scripts only included relevant profile plots, new software had to be created for more advanced analysis.

After the data acquisition, CERN ROOT files are created using analyseall_python2root.sh. This script also separates the data between the device 0 and device 1 data. Then the new ROOT C++

program analysis_xbpf_double_data.cc analyses one dataset and generates the plots.

```
[mraudoni@lxplus061 analysis]$ source analyseall_xbpf_data.sh

Input file 1: data/004/et/D0/out.root

Input file 2: data/004/et/D1/out.root
Name of output files: data_analyzed/004/ET_290
Number of triggers D0: 41971 D1: 41993

Info: Number of Triggers mismatch

Processing... It may take a while.
         0    5    10        20        30        40        50        60        70        80        90        100
Progress: |||||||||||||||||||||||||
```

Figure 4.1 – Analysis of all measurement data with the latest version of the framework

To avoid this repetitive process, the script analyseall_xbpf_data.sh creates new folder and calls analysis_xbpf_double_data.cc with different parameters, creating 32 plots per measurement. (figure 4.1) This process takes several hours, depending on the size of the dataset.

4.3 Trigger Mode Overview

To provide an overview of the implemented hardware trigger modes, this section was added before the introduction to the Virtual Cross Trigger in section 4.4.

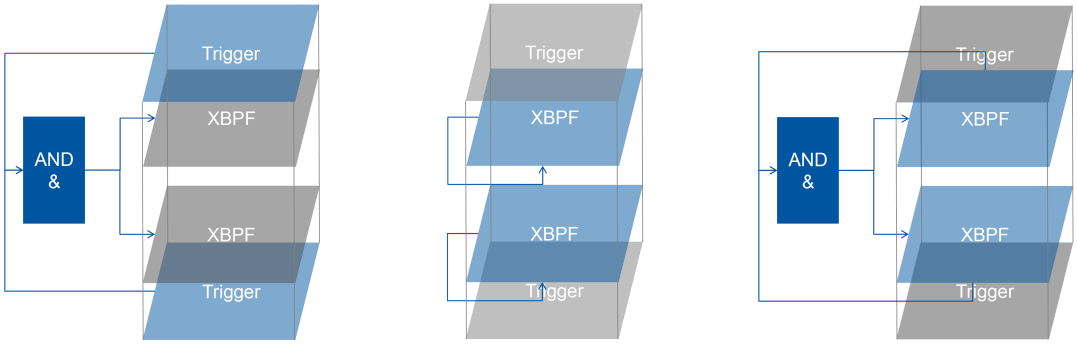

(a) External Trigger (b) Self Trigger (c) Cross Trigger

Figure 4.2 – Trigger mode comparison chart

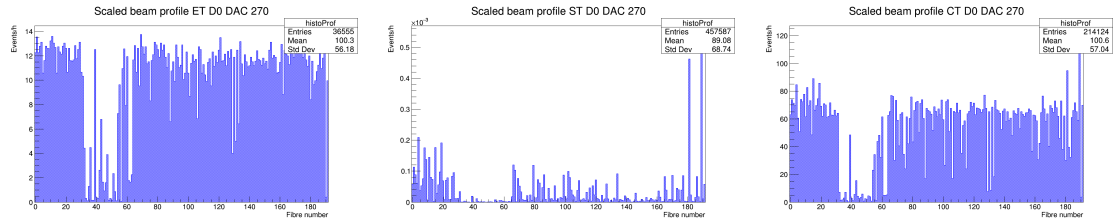

(a) External trigger device 0, 270 threshold (b) Self trigger device 0, 270 threshold (c) Cross trigger device 0, 270 threshold

Figure 4.3 – Trigger profile comparison

4.3.1 External Trigger

The function of the External Trigger (figure 4.2a) is to create a 3-AND coincidence with the ET, which reduces noise. This set-up can verify the functionality of the cross trigger mode.

4.3.2 Self Trigger

The Self Trigger (figure 4.2b) does not use coincidence noise filtering. If there is no beam, the ST profile shows almost exclusively the thermal noise of the channels, as in figure 4.3b. With the low threshold of 270, considerable noise is created, especially on the two channels 181 and 189.

4.3.3 Cross Trigger

The Cross Trigger (figure 4.2c) creates a 2-AND coincidence without external triggers to filter noise. With the low threshold of 270, the high noise of the two channels 181 and 189 alters the beam profile, despite of the AND coincidence.

4.4 Virtual Cross Trigger

The Virtual Cross Trigger is the result of an interpretation of data acquired by External Trigger measurements. The profiles of the Virtual Cross Trigger are not useful for profiling or direct efficiency measurements. The purpose is to simulate and calculate the inefficiencies of a Cross Trigger signal. This can not be done in the Cross Trigger Mode itself, because the baseline for comparison is missing.

4.4.1 Definition

In External Trigger Mode, the XBPFs only acquire data if the trigger signals a passing particle.

Event	$\overline{Device0}$	$Device0$
$\overline{Device1}$	Inefficiency on both devices	Inefficiency on device 1
$Device1$	Inefficiency on device 0	**Efficiency: Virtual Cross Trigger**

Table 4.1 – Logic table of Virtual Cross Trigger coincidence

In case of a trigger signal, there are 4 possible XBPF States. (See table 4.1) If one or both of the devices did not detect a trigger, inefficiency is certain. In case of a detection of both devices, the Virtual Cross Trigger is activated, because the detector in Cross Trigger mode would also trigger.

4.4.2 Analysis Method

```
1  for(UInt_t i=0; i<nentries; i+= quick_div)    // nentries ==
     nentries 2
2  {
3           tree->GetEntry(i);
4           [...]
5         for(UInt_t j=last_offset; j<nentries; j++) // Beginning from
             last offset
6          {
7          tree2->GetEntry(j);
8          if ((ltrigger_msb->GetValue()==ltrigger_msb2->GetValue())
            &&(ltrigger_lsb->GetValue()==ltrigger_lsb2->GetValue()) )
             // time equal
9              {
10              last_offset = j;
11              goto Tmatched;
12             }
13       for(UInt_t j=0; j<last_offset; j++)      // Beginning from 0
          again until the last offset
14       {
15         tree2->GetEntry(j);
```

```
16          if ((ltrigger_msb->GetValue()==ltrigger_msb2->GetValue())
              &&(ltrigger_lsb->GetValue()==ltrigger_lsb2->GetValue()) )
               // time equal
17          {
18            last_offset = j;
19              goto Tmatched;
20  }}}
```

Listing 4.1 – Matching trigger events of two ROOT trees from device 0 and 1

Because the data of both devices needs to be analysed, two files need to be read. To make sure the entries in the ROOT tree are equal, the timestamps are compared and matched, as shown in listing 4.1. For better performance, the `uint last_offset` is saved and the next for-loop starts at this point again to expect the next pair. In case of a match, the data is considered valid and processed further in listing 4.2.

```
1   Tmatched:   // Trigger matched !
2           UInt_t hit=0, hit2=0;
3           for(UInt_t j=0; j<192; j++) // For all fibers
4           {
5               if(lfibre_hits->GetValue(j))  // Device 0 Event
6               {
7               [...]
8                   fibre_activated[hit++]=j; // Post - incrementing
                      hit and saving activated fiber
9               }
10
11              if(multiFlag&&lfibre_hits2->GetValue(j)) // Device 1
                  Event
12              {
13              [...]
14              fibre_activated2[hit2++]=j; // Post - incrementing
                  hit2 and saving activated fiber 2
15              }
16          if(hit&&hit2)       // hits are greater than 0 -> D0 AND D1
              -> VCT
17          {
18            for(UInt_t h=0; h<hit; h++)
19              {
20              [...]
21                  histoProfVCT->Fill(fibre_activated[h]);  // Fill
                      histogram bin of activated fiber
22          }}}
```

Listing 4.2 – Virtual Cross trigger data analysis of matched triggers

After the matching, in the loop `for(UInt_t j=0; j<192; j++)`, events occurred for device 0 `if(lfibre_hits->GetValue(j))` is true. In this case, the array `fibre_activated[]` is filled at

position `UInt_t hit` with the number of the activated fiber. The number of hits is also post-incremented, to count the number of fibers hit in one event and allows the readout of the array. This process is also executed for device 1.

If `(hit&&hit2)` are greater than 0, that means at least one fiber was hit on each plane, which is the definition of the Virtual Cross Trigger. In this case, the VCT histogram is filled.

4.4.3 Simulation and Beam Profile

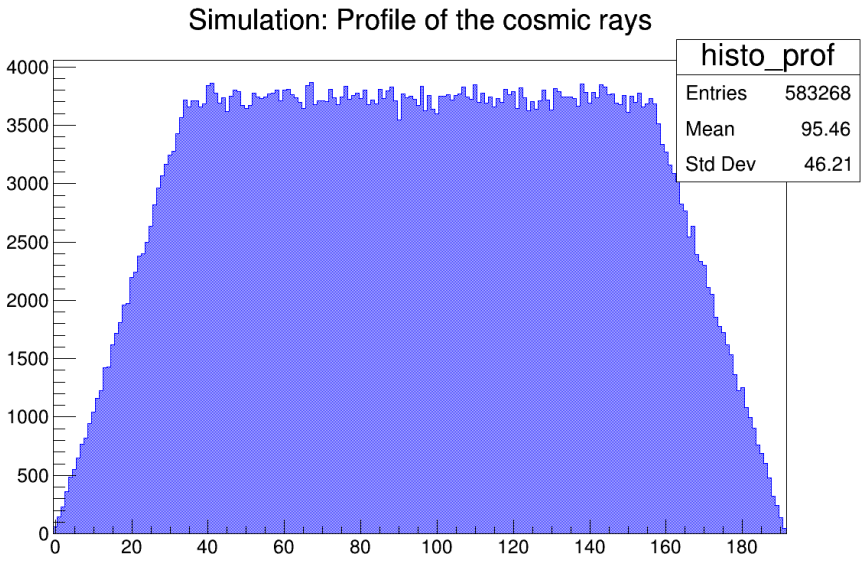

Figure 4.4 – Simulated Beam Profile of device 1, 1 million simulated cosmic rays

Because of the shorter distance between the trigger planes, the resulting cosmic ray profile is expected to be different, because other particle angles are being accepted. Figure 4.4 simulates the resulting cosmic ray profile with one million random cosmic rays.

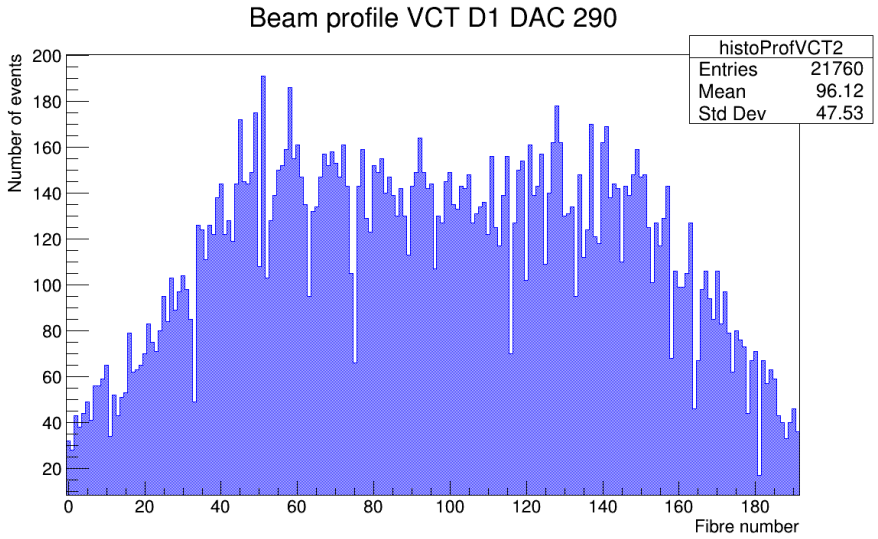

Figure 4.5 – Device 1 Virtual Cross Trigger, threshold 290

The simulation is consistent with the measurement in figure 4.5, apart from inefficient channel variations.

4.4.4 Combination of beam profiles

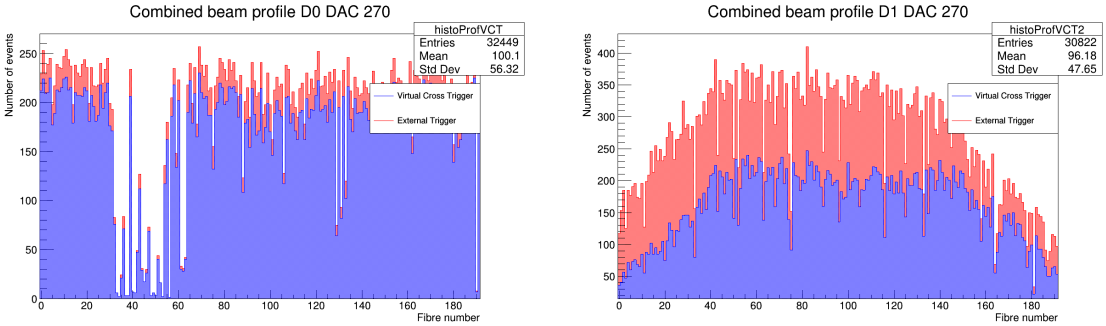

(a) Device 0, threshold 270

(b) Device 1, threshold 270

Figure 4.6 – Device 0 and 1 Virtual Cross Trigger compared to the External Trigger profile

In figure 4.6, ET and VCT profiles are plotted on the same canvas.

Upon interpretation as a stacked histogram, the blue candles represents the efficiency of the VCT, while the red candles would represent its inefficiency.
To make beam profiles more comparable, the analysis framework was adapted to output plots scaled to the duration of the measurement. This is implemented by scaling the y-axis to events per hour.

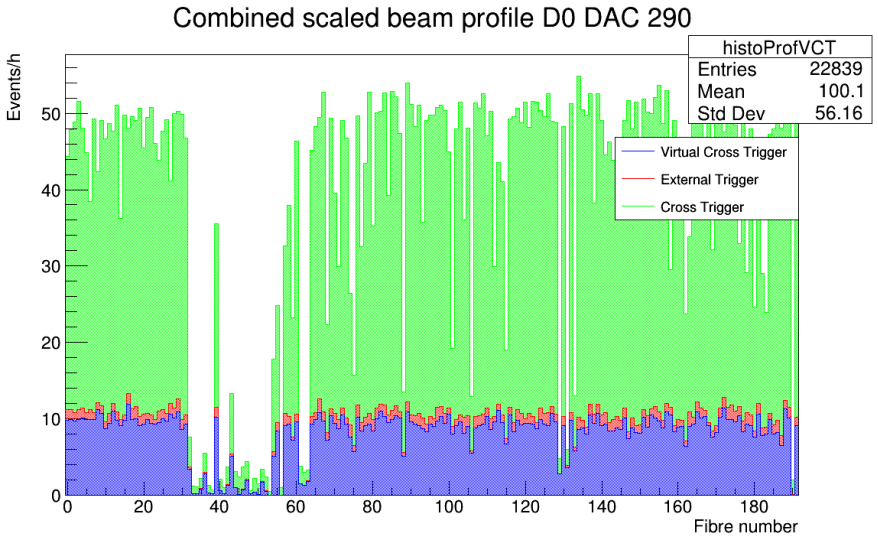

Figure 4.7 – Combined beam profile on device 0, threshold 290.

In figure 4.7, ET, CT and VCT cosmic muon profiles are scaled and plotted in one canvas. The inefficient channels are consistent between all 3 measurements and the plots look comparable. However, the CT has a much higher event rate than both the ET and the VCT. This is further explained in section 4.4.5.

Note: On plots 4.6a, 4.7 and following, fibers 32 until 64 are detecting less events due to a problem with the second CITIROC ASIC. For efficiency calculations, these channels were masked and the number of hits compensated by multiplication with $\frac{6}{5}$.

4.4.5 Efficiency considerations

In plot 4.6a, the VCT inefficiency loss is very small, compared to the device 1 plot. This could mislead to the interpretation, that device 0 is more efficient than device 1. The right interpretation is that the inefficiency of one device prevents the other device in CT mode to detect existing particles.

Event	$\overline{Device0}$	$Device0$
$\overline{Device1}$	16.35% Inefficiency on both devices	14.76% Inefficiency on device 1
$Device1$	31.28% Inefficiency on device 0	**37.61% Efficiency: Virtual Cross Trigger**

Table 4.2 – Logic table of VCT efficiency measurement at threshold 270

The (in-)efficiencies for this measurement with masked channels 32-64 and threshold 270, computed by the created measurement framework are presented in logic table 4.2.

It may surprise the audience that in figure 4.7, the CT profile has a much higher event rate than

the ET and VCT. This is expected in consideration of the efficiency relations of these individual trigger modes.

$$\epsilon_{ETD0} = \epsilon_{upperET} * \epsilon_{XBPFD0} * \epsilon_{lowerET} \tag{4.1}$$

$$\epsilon_{ETD1} = \epsilon_{upperET} * \epsilon_{XBPFD1} * \epsilon_{lowerET} \tag{4.2}$$

The efficiency of the external trigger mode is the product of the efficiency of the XBPF device and the both trigger planes.

$$\epsilon_{VCTD0} = \epsilon_{upperET} * \epsilon_{XBPFD0} * \epsilon_{XBPFD1} * \epsilon_{lowerET} \tag{4.3}$$

$$\epsilon_{VCTD1} = \epsilon_{upperET} * \epsilon_{XBPFD0} * \epsilon_{XBPFD1} * \epsilon_{lowerET} \tag{4.4}$$

The efficiency of the virtual cross trigger mode is the product of the efficiency of both XBPF devices and the both trigger planes. This means a four-way AND coincidence is created, which ensures the particle is not noise. However, all the inefficiencies of the four devices are multiplicated.

$$\epsilon_{CTD0} = \epsilon_{XBPFD0} * \epsilon_{XBPFD1} \tag{4.5}$$

$$\epsilon_{CTD1} = \epsilon_{XBPFD0} * \epsilon_{XBPFD1} \tag{4.6}$$

The efficiency of the cross trigger mode is only the product of the efficiency of the XBPF device. This explains the high event rate and efficiency in figure 4.7.

4.4.6 Noise considerations

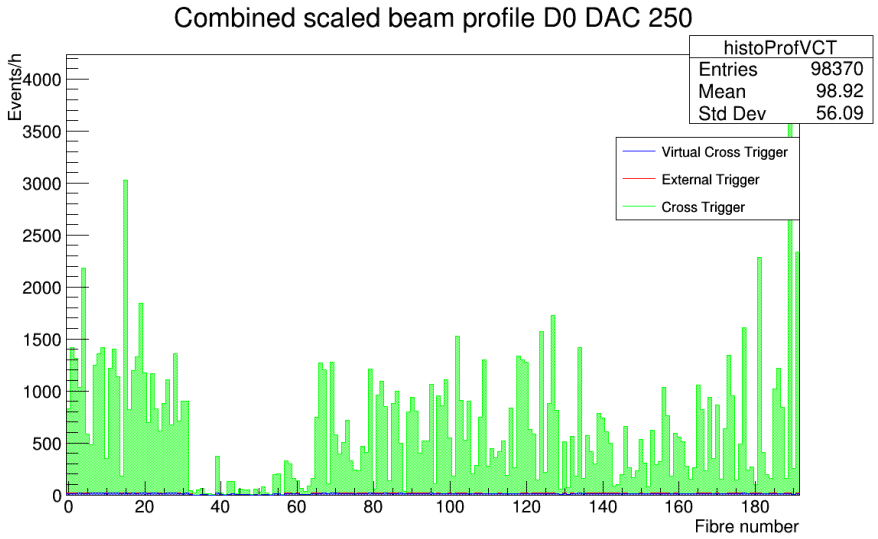

Figure 4.8 – Combined beam profile on Device 0, threshold 250.

At low threshold values like 250, the noise is to high to be cancelled by the 2-AND coincidence. The noise causes the CT measurement to reach noise event rates magnitudes higher than the cosmic muons. (figure 4.8)

Note: Since the VTC is not investigating noise because of its 4-way coincidence, the rate is still lower than the external trigger. Both of these rates are not visible in image 4.8 because they are too weak.

4.5 Measurements with Oscilloscope

An other way of measuring the efficiency of the system is a manual measurements of the LEMO outputs L3 and L4 of the VFC Backend. Therefore, the VFC Backend output registers L3FLAGSRC and L4FLAGSRC were configured to 0x3 and 0x7. This configures the output multiplexer, which is equal to the ST/CT multiplexer to output the OR of both devices to the L3 connector and the AND of both devices to the L4 connector.

Figure 4.9 – Measuring coincidence signals with Teledyne Lecroy Waverunner oscilloscope at the VFC Backend

The output of the L3 and L4 connectors is connected to the oscilloscope with the ET signal as the trigger source. (figure 4.9)

The oscilloscope measurements were meaningful to the validation process of the complex XBPF system, because the signal properties and effects are hidden by the abstraction levels of the signal processing system.

4.5.1 Signal Measurements

During the signal measurement, the widths of the channels and the number of (trigger) signals is measured. Yellow channel C1 is connected to the ET as the trigger source. Red C2 is connected to the L3 output, which represents the multiplexed OR of both XBPF devices. Blue C3 is connected to the L4 output, which represents the multiplexed AND. In figure 4.10, the signal shows efficiency at both devices, since the blue C3 signal is activated. Upon interpretation of the signals L2 (OR) and L3 (AND), the original signals can be restored. The

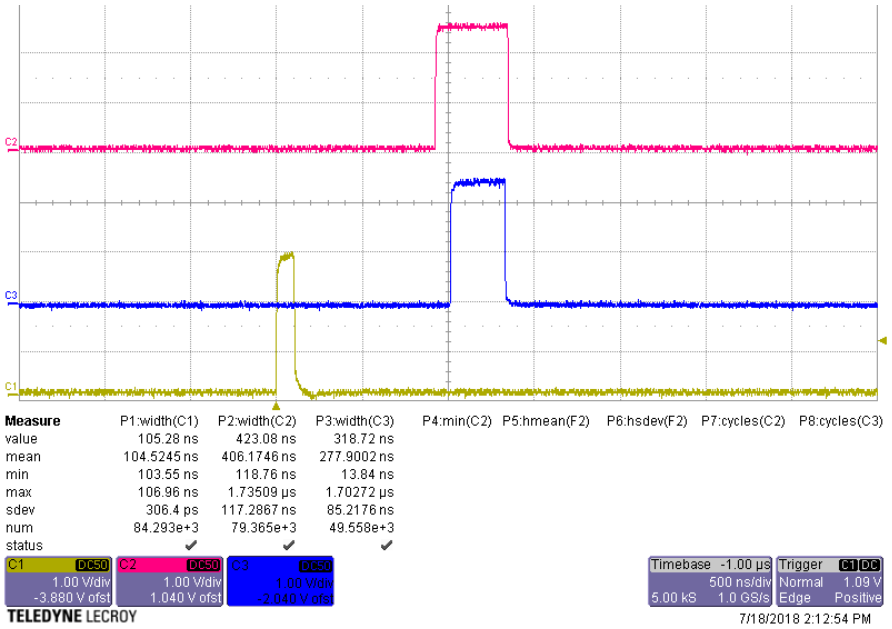

Figure 4.10 – Coincidence signal measurement, threshold 290.

signal of one device starts with the rising edge of C2 and stops with the falling edge of C3. The other signal starts at the rising edge of C3 and stops at the falling edge of C2. This is due to the fact that both signals have to be included in the duration of the C2 signal, while their overlap is the duration of C3.

This measurement helped validate the XBPF system and revealed a wrong setting of the DXSETFLAGWITH register at measurements 001-003.

4.5.2 Efficiency Measurements

The num-counters for the signals C1,C2 and C3 measure the efficiency of the device. The number of triggers from the C1 ET is the baseline for the number of muons detected. $\frac{C3}{C1}$ equals the efficiency of both devices (AND), which should resemble the performance in CT mode. $\frac{C1-C3}{C1}$ equals the inefficiency of one or both devices (NAND) and $\frac{C2-C3}{C1}$ equals the (in)efficiency on exactly one of the two devices (XOR). $\frac{C1-C2}{C1}$ equals the total inefficiency of both devices (NOR).

This test was repeated for thresholds 250-290 parallel to the main profile measurements. On low thresholds, the efficiency is very high due to the many DCE. Because the oscilloscope counts all the rising edges in the frame, also signals without a trigger (noise) may be counted. This is a predictable measurement error. Also, the measurements were taken on different days with different ambient variables, especially temperature. At threshold 280, the significant efficiency drop is expected to be due to a measurement error.

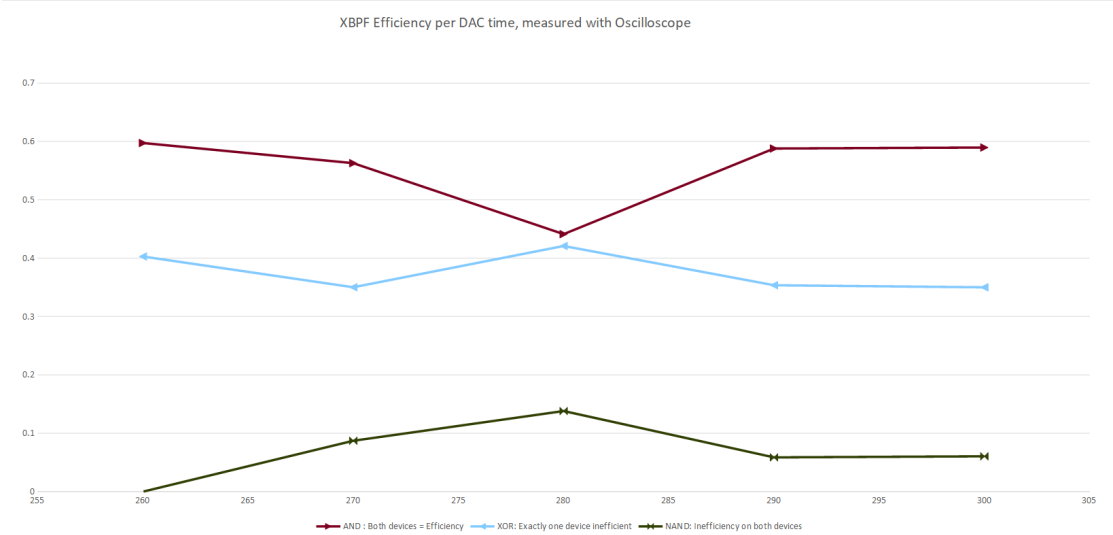

Figure 4.11 – MS Excel computed XBPF CT (in-)efficiencies, thresholds 250-290

At high threshold levels, the efficiency is at 59%, which is beneath the expectation, due to an error in the testbench setup.

4.6 Vector analysis

Because both XBPF Frontends fibers are in parallel, the angle of the particles can be determined by the trigonometric equation 4.7

$$\Phi = tan^{-1}\left(\frac{x_{Device0-Device1}[mm]}{(Fiber_{D0} - Fiber_{D1}) \cdot 1mm}\right) \tag{4.7}$$

In this version of the analysis framework, the distance of the fibers $Fiber_{D0} - Fiber_{D1}$ is plotted instead of the resulting angle.

4.6.1 Results

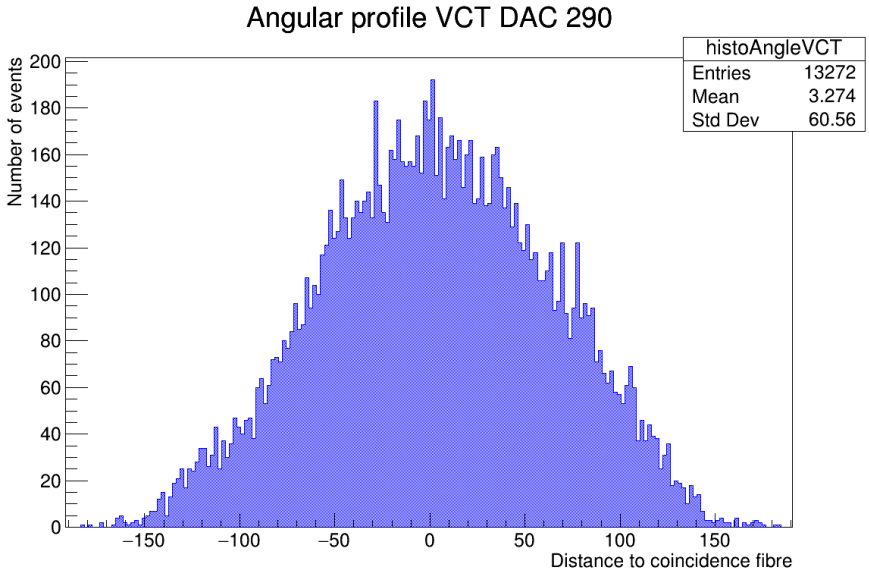

Figure 4.12 – VCT angular profile, threshold 290.

The resulting angular profile (figure 4.12) matches a cos^2 function, which is expected due to the geometric setup.
The histogram shows a small shift to the right (positive fiber distance) and a peak at a distance of about +75. The mean of the distance is +3.2. This can not be explained due to a misalignment, because the XBPF fiber planes are carefully guided by a metal frame.

Looking at the regular beam profile (figure 4.13) of device 1, which is on the upper side, another anomaly can be observed, marked in red. The mean (90.5 instead of 95.5) of this profile is shifted to the left with the peak clearly at fiber 50.

Looking at the geometry of the testbench, (section 2.5.1) an explanation is found: Because

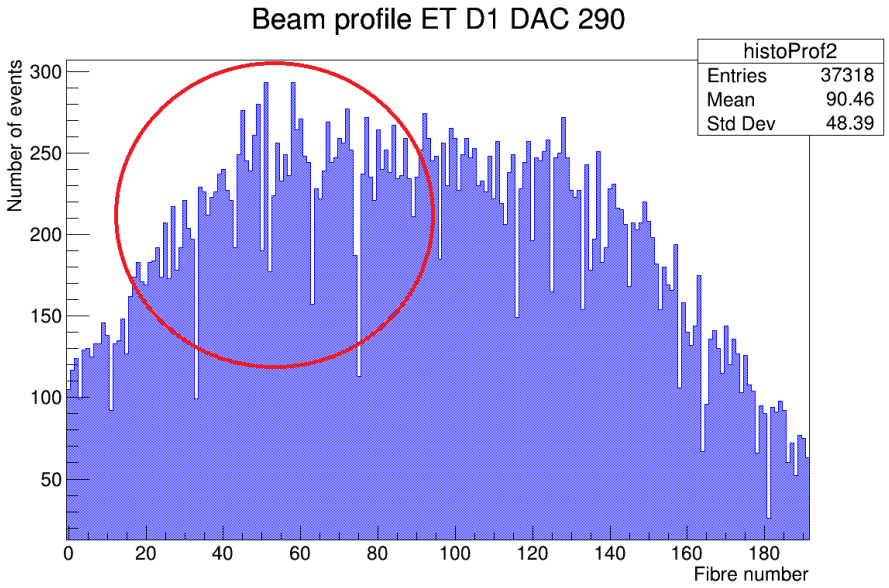

Figure 4.13 – Beam profile device 1, threshold 290.

the upper external trigger is tilted 90°, the fibers are leaving the active area to the detector extend to the "left" (low fiber count) side of the XBPF. Because these fibers also detect passing particles, particles can activate the upper ET entering "left" of the active area. This is detected by the peak on the "left" fibers 20-80 and the shifted mean of the upper device 1. The angular profile shifted towards positive angles completes the verdict: At the upper detector more events are detected on low fiber counts and the angle of detection is more positive, because of the overlapping upper ET.

This is an effect of the cosmic testbench and will not occur in the regular beamline. This effect explanation proves the general functionality of the system and the correctness of the analysis.

4.6.2 Continuity analysis

This vector analysis was also analysed in two dimensions against the number of events. This could maybe have revealed a cosmic ray source by angular difference over time by the rotation of the earth. In figure 4.14, no diagonal lines were strong enough to be considered a detection. At the lower threshold 250, the noise dominates the signal, which results in a clearer cos^2 function.

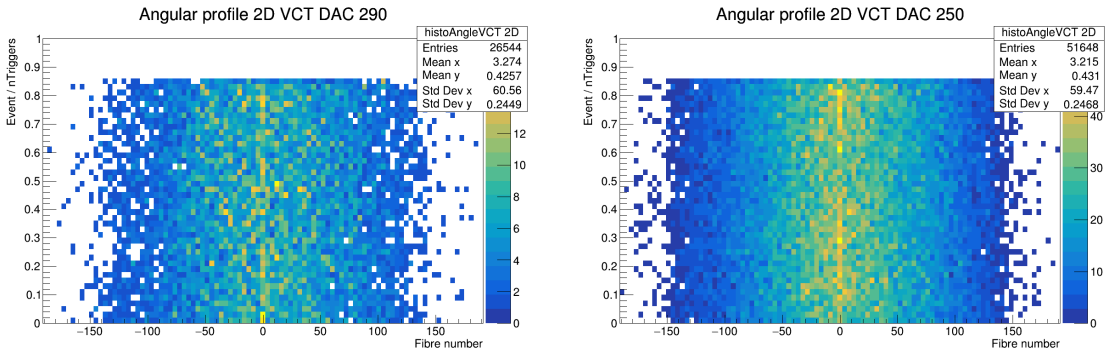

(a) Threshold 290

(b) Threshold 250

Figure 4.14 – Two-dimensional vector analysis over the number of events

4.7 Moving Source Test

For this test, a Strontium^{90} source with 21Mbq of 0.546 MeV β^- decay was put on top of the cosmic test bench near the close edge. Every 10 seconds the source was moved until the rear end of the black box.

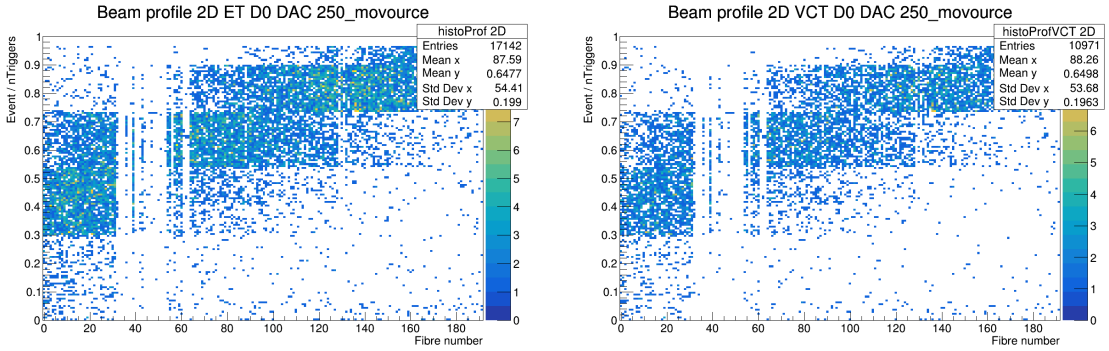

(a) External Trigger

(b) Virtual Cross Trigger

Figure 4.15 – Two-dimensional beam profiles during moving source test

4.8 System efficiency calculations

The analysis framework saved, apart from plots, text files with fiber counts, debug information and efficiency calculations. These calculations were collected and further abstracted with MS Excel.

Note: Fibers 32 until 64 are detecting less events due to a problem with the second CITIROC ASIC. For system efficiency calculations, these channels were masked and the number of hits compensated by multiplication with $\frac{6}{5}$.

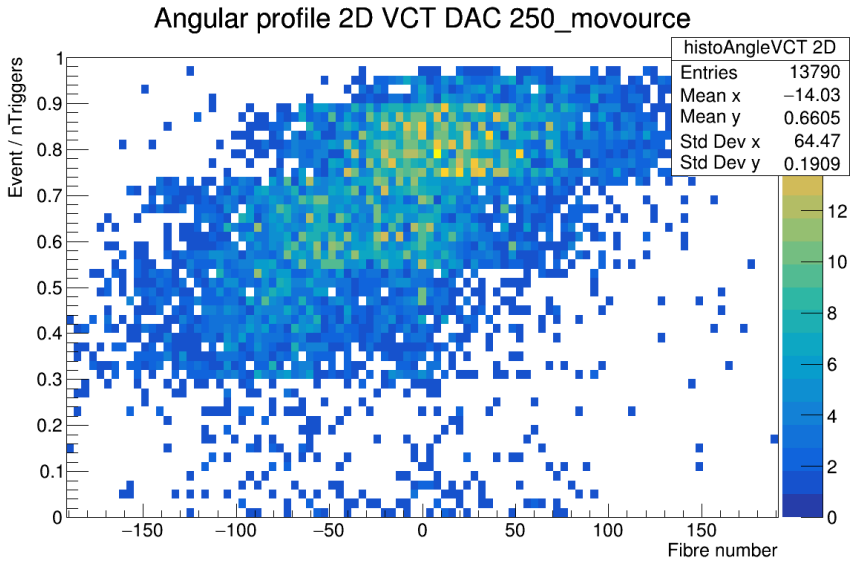

Figure 4.16 – Angular beam profile over the number of triggers during moving source test

Figure 4.17 shows the event rate for measurements across the thresholds. Below the threshold of 280, the CT detects too many events, which shows the vulnerability against this big DCR.

To calculate the isolated efficiency of all planes of the detector, the number of the actual arrived muons (baseline) must be known.

$$\epsilon_{VCTD0} = \epsilon_{CTD0} * \epsilon_{ET} \tag{4.8}$$

The 4-AND coincidence VCT efficiency is the product of the 2-AND CT coincidence efficiency

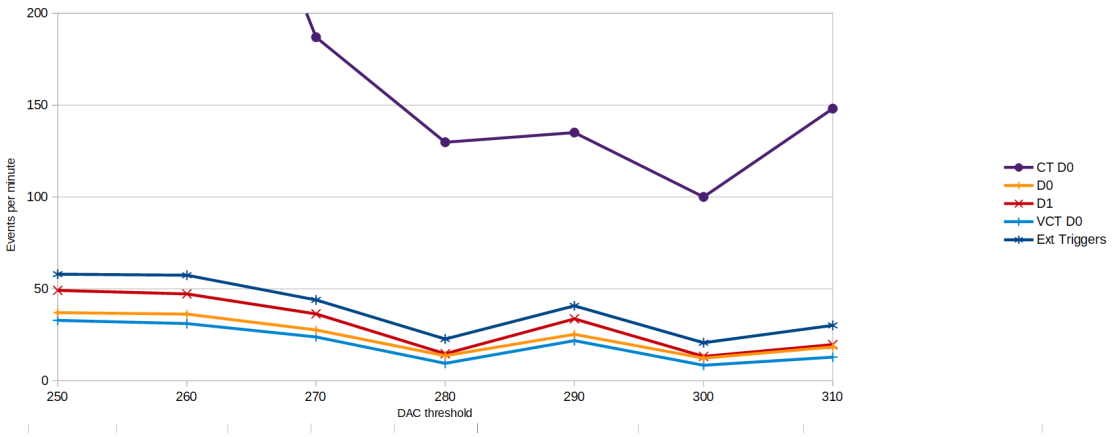

Figure 4.17 – Events per minute, thresholds 250-310

and the 2-AND coincidence of the external trigger planes. (equation 4.8)

$$\frac{VCTD0}{X_{baseline}} = \frac{CTD0}{X_{baseline}} * \frac{ET}{X_{baseline}} \qquad \epsilon_{Device} = \frac{events}{X_{baseline}} \tag{4.9}$$

$$X_{baseline} = \frac{CTD0 * ET}{VCTD0} \tag{4.10}$$

Equation 4.9 applies the baseline definition to 4.8 and comes to the result (equation 4.10), that the baseline can be directly calculated with the rates of the three event rates.

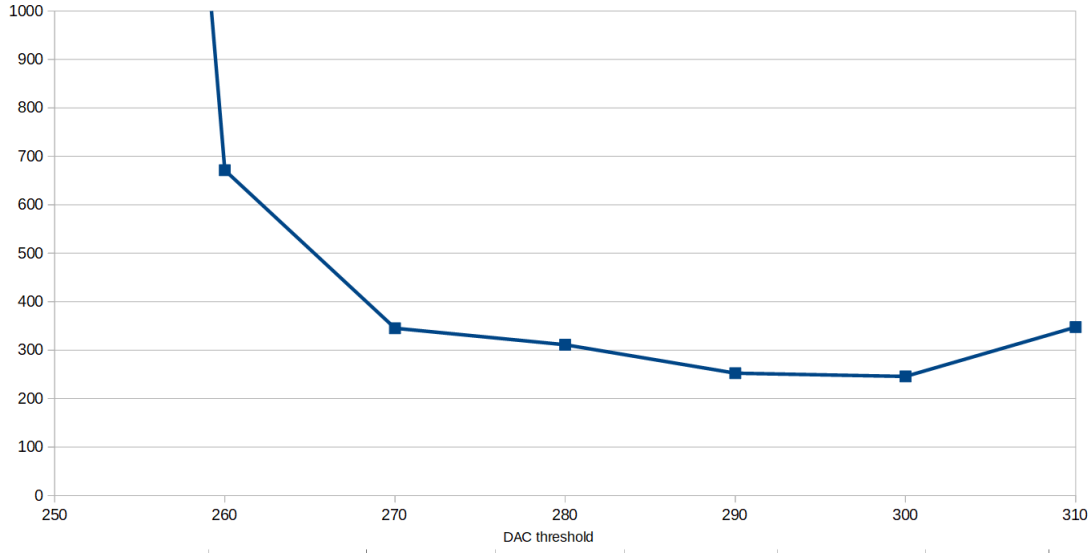

Figure 4.18 – Cosmic muon detection rate calculated baseline, thresholds 250-310

In figure 4.18, the muon baseline is plotted for the different thresholds. Because of the noise limitations, the measurements below 270 should not be considered. This leads to an estimated baseline rate of 200-400 events per minute.

The average muon flux at sea level is about 1 muon per square centimetre per minute. [18] [19] With an active area of 192mm x 192mm, the area is 368 square centimetres, which equals to a rate of 368 muons per minute.

This confirms the calculations based on the measurements.

The baseline allows the direct calculation of the efficiency from the event rate. (equation 4.8) In figure 4.19, the measured efficiencies are plotted on the same canvas as the product of isolated efficiencies, dependent on the baseline and threshold. This shows that the XBPF in CT Mode is more efficient than one of two external triggers. The calculated efficiencies of $\epsilon_{D0} \cdot \epsilon_{D1}$ (dark blue) are almost identical to the measured CT efficiency.

However, the calculated efficiencies are not meeting the expectations because of an error in the testbench setup.

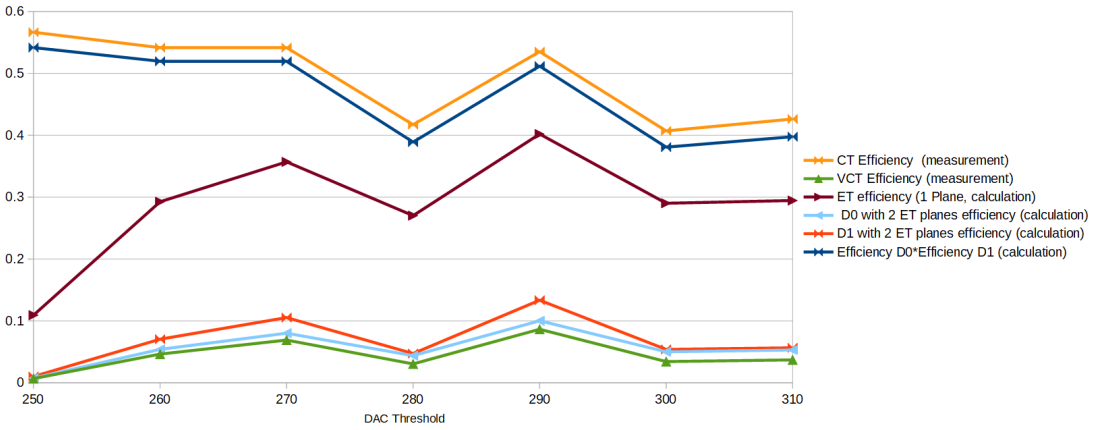

Figure 4.19 – Measured and calculated efficiency, thresholds 250-310

4.9 Cross Trigger continuity analysis

To investigate the stability and consistency of the system, the profiles of the dataset were plotted in two dimensions.

4.9.1 2D Plotting against the number of events

Because a one-dimensional histogram only reveals the sum of events per bin, the time factor is not analysed. Because of the successful test of the timing of the Cross Trigger in the order of (nano-) seconds, the macroscopic timeframe was also investigated. The analysis against the number of the event could reveal, for example, oscillating temperature correction factors of the frontend electronics.

```
1 TH2F* histoProf2D = new TH2F("histoProf 2D", "Beam profile D0 2D",
    192, -0.5, 191.5, 150, 0, 1);
2 [...]
3     for(UInt_t j=0; j<192; j++)
4     {
5     [...]
6     histoProf2D->Fill(j,((float) quick_div*(float) matchedTriggers)
        /(float) nentries);
7     }
```

Listing 4.3 – Filling histogram for two-dimensional plotting against the numbers of triggers in analysis_xbpf_double_data.cc

The plot was created from a two-dimensional histogram of the ROOT class "TH2F". In line 6 of the listing 4.3, the histogram is filled with the fiber number on the first dimension and the number of triggers.

The continuity analysis against the number of triggers in figure 4.20 did not reveal any anoma-

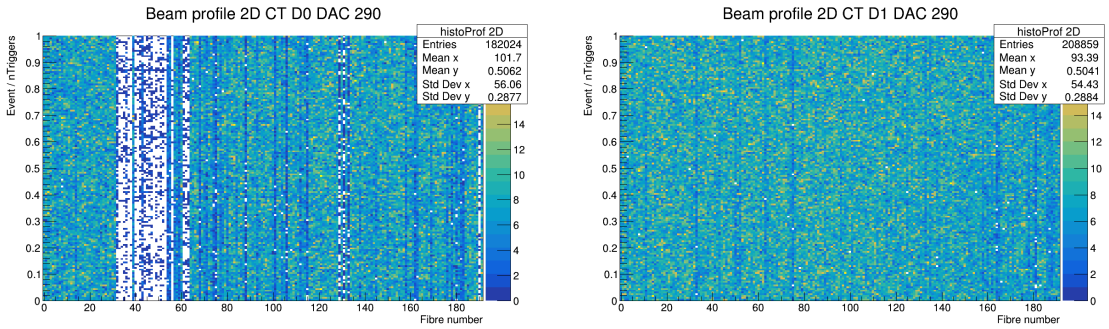

(a) Device 0, 290 threshold

(b) Device 1, 290 threshold

Figure 4.20 – Cross Trigger two-dimensional profile of XBPF Devices 0,1 at threshold 290

lies.

4.9.2 2D Plotting against the passed time

```
1     TH2F* histoProft2D = new TH2F("histoProf t 2D", "Beam profile
        D0 2D", 192, -0.5, 191.5, 150, 0,  (UInt_t) meastime+1);
2  [...]
3     for(UInt_t j=0; j<192; j++)
4     {
5     [...]
6     histoProft2D->Fill(j, (float) ((UInt_t) (ltrigger_msb->GetValue
        ()-tfirst_trigger)/60));
7     }
```

Listing 4.4 – Filling histogram for two-dimensional plotting against the passed time in analysis_xbpf_double_data.cc

The plot was created from a two-dimensional histogram of the ROOT class "TH2F" with the bin boundaries set on runtime. In line 6 of the listing 4.3, the histogram is filled with the fiber number on the first dimension and the time in minutes, typecasted to a float datatype.

In the plots 4.21a, 4.21b and others, the measurement does not show any anomalies considering continuity. In the plots 4.21c and 4.21d however, the plots for both devices show anomalies. Around minute 140, the number of events decreased considerably. This can be explained by the manual interruption of the measurement, visible in the raw data, from 14:42 to 14:58.

At the times of 550-625, 675-900 and 1000-1200 the intensity is slightly reduced (visible as blue horizontal lines) An explanation for these anomalies is to be found. A temporary decrease in the cosmic muon flux is unlikely.

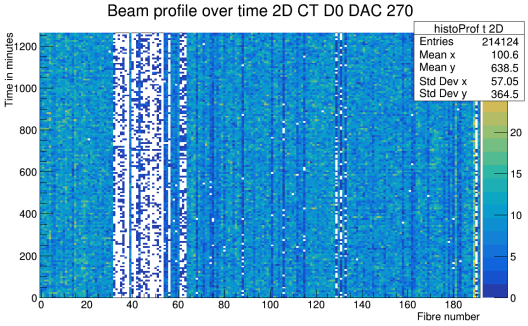

(a) Device 0, 270 threshold

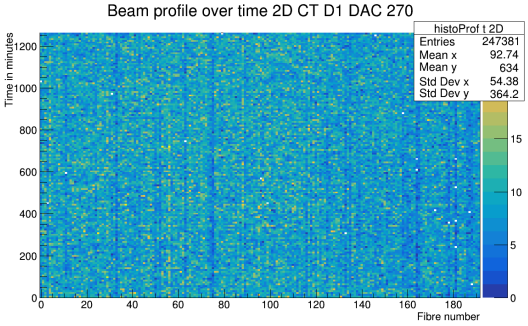

(b) Device 1, 270 threshold

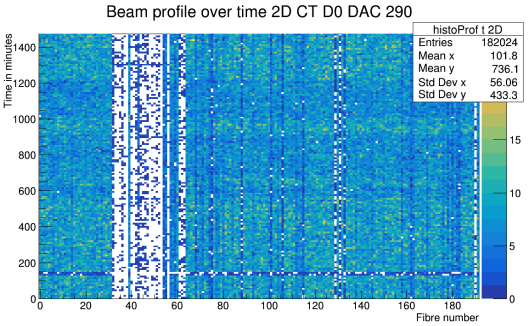

(c) Device 0, 290 threshold

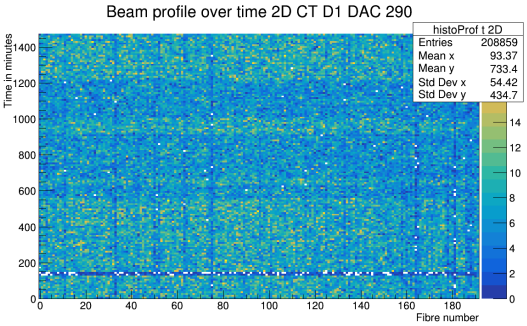

(d) Device 1, 290 threshold

Figure 4.21 – Cross Trigger continuity analysis of XBPF devices 0,1 at thresholds 270 and 290. Plots c,d showing intensity abnormalies

5 Resumé and outlook

The XBPF Technology has the potential to become the low intensity beam profile monitor of the future.
The new channel masking features allow faulty channels to be masked remotely to avoid the malfunction of the whole system, which is crucial in the inaccessible radioactive environment of the beamline. The novel Self Trigger and Cross Trigger modes allow measurements without an external trigger, which is very important for beam commissioning. Colleagues from Beam Operations (BE-OP) indicated they were "very happy" with the new modes.
The Cross Trigger performs very well in noise cancellation and efficiency comparisons. At the desired threshold of 290, the thermal noise is cancelled while the combined detection efficiency of both planes peaked at 53.5%.
Another advantage of the Cross Trigger Mode is the profile of the beam as-is, without any unwanted geometric effects from external trigger planes.

The developed data analysis framework is available through CERN GitLab which includes many new XBPF analysis methods, like continuity, vector and scaled analysis. The Virtual Cross Trigger is a new analysis method which reveals the efficiency correlation and effects between the cross-triggered devices.

In the end of August 2018, the matter of this thesis has to face the application test in the EHN1 tertiary beam line to push fundamental neutrino research.

5.1 CERN Experimental Areas

In the North Area, the SPS beam is slow extracted [1] to a target to create a secondary beam. This beam consists of particles that were created by the interaction of the primary beam with the target. The secondary and tertiary beam is less intense and energetic, which makes it suitable for beam profiling with scintillating fibers.

[1] Nearly constant particle extraction without bunching

Figure 5.1 – Protodune neutrino detector assembly area in the new section of the north hall. Credit: CERN

The new Neutrino Platform in the North Area (see figure 5.1) is being constructed (September 2018) to contribute to fundamental neutrino physics at CERN. [20]

The beam profiles for the new protoDUNE neutrino experiment will be created using the XBPF Beam Monitors. [21]

5.2 Beam-line application

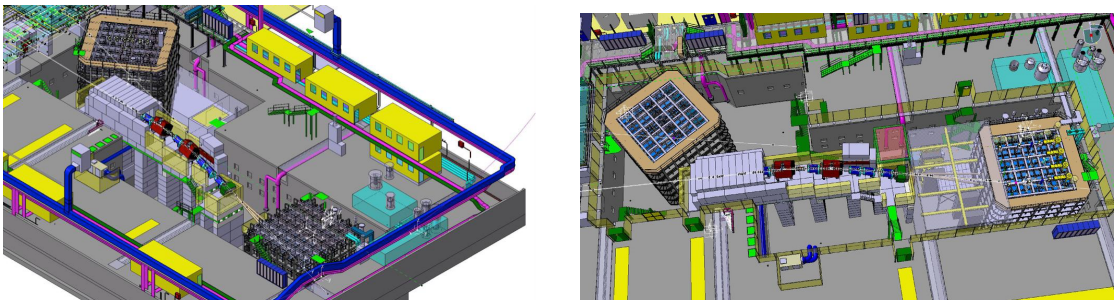

Figure 5.2 – Views of the EHN1 tertiary beam line to the Neutrino Platform. [21]

In August 2018, the system is being installed and commissioned in the very low intensity beamline in the new EHN 1 Extention H2 of the north hall. (see figures 5.2 and 5.3)

The very low intensity beam is incoming from the right side of the figures 5.2 and 5.3. By bending with dipole magnets (blue), the desired particles are separated and diverted, instead of hitting the beam dump. The profile and timing will be measured by four XBPF Systems (purple) with three externals triggers (green), as visible in picture 5.3.

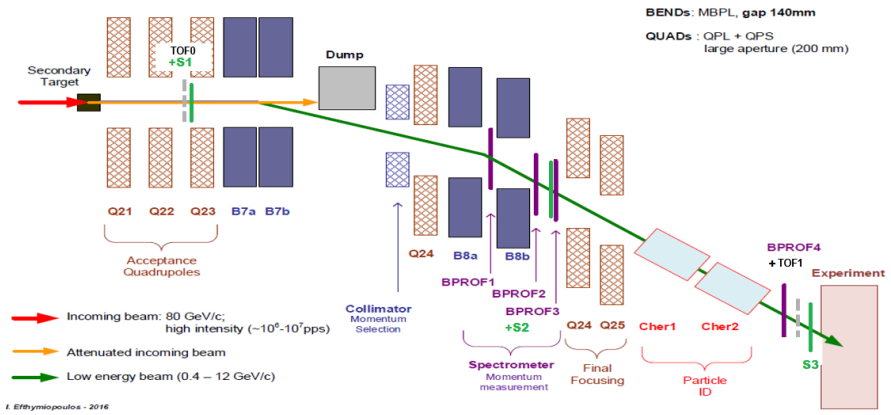

Figure 5.3 – EHN 1 Extension H2 VLI Beam Shematic Layout [16]

The beam commissioning phase starts at the end of August 2018.

Figure 5.4 – Inspection of the XBPF installation slots BPROF2, BPROF3 (covered by silver foil) in front of the Q24 focusing magnet of the EHN1 tertiary beam line with the author.

5.3 Cosmic Telescope

The cosmic testbench, in figure 2.5, is designed to calibrate the system with cosmic muons. With the two XBPF Frontend Boards, one - dimensional angular profiles were created. By using the same configuration with two 90°- rotated XBPF Frontend pairs, the three-dimensional vector of the particle can be detected. The angular resolution can be improved by separating

the plane pairs. By pointing the Cosmic Telescope at a big mass, the number of detected muons is expected to decrease due to absorption. The resulting rendering (Muon Tomography) could reveal denser and lighter matter, comparable with X-Ray Radiography.

By adding a dipole magnet in between 4 XBPF Pairs, particle spectroscopy is also possible.

A Appendix

Listing A.1 – Measurement log with comments. DAC refers to the setting of the treshold DAC in the CITIROC ASIC

```
Generation 1:
-------------------------------------------------------------------------------

#001:
et Temperature 37.1 deg, DAC 290
st Temperature 37.5 deg, DAC 290
ct Temperature 37.5 deg, DAC 290 - end: 37.0 deg
#002:
st Temperature 37.0 deg, DAC 270, d0:160e/s d1:900e/s
ct Temperature 37.0 deg, DAC 270,
et Temperature 36.4 deg, DAC 270, d0:11e/s d1:11e/s
#003: DAC 250
st Temperature 35.2 deg, d0:10.000e/s d1:30.000/s
ct Temperature 38.8 deg, d0:e/s d1:e/s  (problem with timings: Now flagwith = 13)
et Temperature 35.2 - 34.5 - 36.8 deg, d0:10e/s d1:10e/s (3Days)

Generation 2:
-----------------------------------------------------------------------------------------


004 New setup with stable power DAC 290 flagwith 0xf
et Temperature 36.6 deg, d0:1e/s d1:1e/s        MISSING&found
st Temperature 39.8 deg, d0:400e/s d1:40e/s
ct Temperature 39.8 deg, d0:3e/s d1:3e/s

005 DAC 270
st Temperature 39.3 deg, d0:5000e/s d1:100e/s
ct Temperature 39.3 deg, d0:3,2e/s d1:3,2e/s
et Temperature 40.4 deg, d0:0.7e/s d1:0.7e/s

006 DAC 250
st Temperature 40.0 deg, d0:50000e/s d1:20000e/s
ct Temperature 40.0 deg, d0:50e/s d1:50e/s
ct Temperature 41.2 deg, d0:11e/s d1:11e/s

007 DAC 260
st Temperature 38.5 deg, d0:5000e/s d1:400e/s
ct Temperature 38.5 deg, d0,1:6.7e/s
```

```
et Temperature 39.8 deg, d0:e/s d1:e/s

Generation 3:
-------------------------------------------------------------------------------------

008 DAC 280     // fault here
st Temperature 39.3 deg, d0:40e/s d1:30e/s
ct Temperature 39.3 deg, d0,1:1.8e/s
et Temperature 42.0 deg, d0:<1e/s d1:1e/s

008b DAC 280
et Temperature 41.5 deg, d0:<1e/s d1:1e/s

111 Mask measurement with DAC 260

112 DAC 290 - small source
et Temperature 41.5 deg, d0:25e/s d1:25e/s

009 DAC 300
et Temperature 42.0 deg, d0:<1e/s d1:1e/s
st Temperature 38.8 deg, d0:173e/s d1:30e/s
ct Temperature 38.8 deg, d0:2e/s d1:2e/s

113 DAC 250: OSCI Noise measurement (short time)
st Temperature 40.6 deg, d0:35000e/s d1:20579e/s
ct Temperature 40.6 deg, d0,1:45e/s

010 DAC 310:
et Temperature 40.6 deg, 0.6 e/s
ct Temperature 37.9 deg, 1.6 e/s (short)
st Temperature 37.9 deg, d0: 70 d1: 30 e/s (short)

011 DAC 250: repetition
st Temperature 38.8 deg, d0: 30000 d1: 2000 e/s
ct Temperature 38.8 deg, d0: 40  e/s

114 DAC 250: big moving source measurement
et Temperature 40.6 deg

013 DAC 260: repetition short
ct Temperature 40.6 deg, d0: 1  e/s

015 DAC 280 : rep
et Temperature 42.3 deg, d0: 1  e/s (first, temperature correction was disabled)
st Temperature 42.3 deg, d0: 242 d1: 37  e/s
```

Bibliography

[1] T. White, "Scintillating fibres", *Nuclear Instruments and Methods in Physics Research Section A: Accelerators, Spectrometers, Detectors and Associated Equipment*, vol. 273, no. 2-3, pp. 820–825, 1988.

[2] I. Ortega Ruiz, "Accurate profile measurement of the low intensity secondary beams in the cern experimental areas", *EPFL Infoscience*, p. 204, 2018.

[3] Hamamatsu Photonics, *S13360-1350cs mppc for precision measurement*, http://www.hamamatsu.com/us/en/S13360-1350CS.html, Accessed on 2018-08-13.

[4] B. F. Aull, A. H. Loomis, D. J. Young, R. M. Heinrichs, B. J. Felton, P. J. Daniels, and D. J. Landers, "Geiger-mode avalanche photodiodes for three-dimensional imaging", *Lincoln Laboratory Journal*, vol. 13, no. 2, pp. 335–349, 2002.

[5] S. Cova, M. Ghioni, A. Lacaita, C. Samori, and F. Zappa, "Avalanche photodiodes and quenching circuits for single-photon detection", *Applied optics*, vol. 35, no. 12, pp. 1956–1976, 1996.

[6] LHCb Collaboration and others, "Lhcb tracker upgrade technical design report", CERN, Tech. Rep., 2014.

[7] Ketec GmbH, *Device parameters photon detection efficiency*, https://www.ketek.net/sipm/technology/device-parameters/, Accessed on 2018-08-13.

[8] Hamamatsu Photonics, *Mppcs for precision measurement s13360 series*, http://www.hamamatsu.com/resources/pdf/ssd/s13360_series_kapd1052e.pdf, Accessed on 2018-08-13.

[9] P. Lightfoot, G. Barker, K. Mavrokoridis, Y. Ramachers, and N. Spooner, "Characterisation of a silicon photomultiplier device for applications in liquid argon based neutrino physics and dark matter searches", *Journal of Instrumentation*, vol. 3, no. 10, P10001, 2008.

[10] Weeroc SAS, *Citiroc 1a front-end asic*, https://www.weeroc.com/en/products/citiroc-1a, Accessed on 2018-08-13.

[11] J. Fleury, S. Callier, C. de La Taille, N. Seguin, D. Thienpont, F. Dulucq, S. Ahmad, and G. Martin, "Petiroc and citiroc: front-end asics for sipm read-out and tof applications", *Journal of Instrumentation*, vol. 9, no. 01, p. C01049, 2014.

[12] S. Callier, C. D. Taille, G. Martin-Chassard, and L. Raux, "Easiroc, an easy & versatile readout device for sipm", *Physics Procedia*, vol. 37, pp. 1569–1576, 2012.

[13] G. Pareschi, G. Agnetta, L. Antonelli, D. Bastieri, G. Bellassai, M. Belluso, C. Bigongiari, S. Billotta, B. Biondo, G. Bonanno, *et al.*, "The dual-mirror small size telescope for the cherenkov telescope array", *arXiv preprint*, 2013.

[14] J. Serrano, M. Lipinski, T. Wlostowski, E. Gousiou, E. van der Bij, M. Cattin, and G. Daniluk, "The white rabbit project", 2013.

[15] CERN - BE, *Vme fmc carrier hpc-ddr3 (vfc-hd)*, https://www.ohwr.org/projects/vfc-hd/, Accessed on 2018-08-13.

[16] I. Ortega, *Accurate profile measurement of the low intensity secondary beams in the cern experimental areas - public defense*, https://indico.cern.ch/event/678621/attachments/1610907/2557875/phd_public_defence_Inaki_Ortega.pdf, Accessed on 2018-08-13.

[17] J. Kral and M. Raudonis, "Xbpf measurement modes and communication (draft)", CERN BE-BI-PI, Tech. Rep., 2018.

[18] N. Ramesh, M. Hawron, C. Martin, and A. Bachri, "Flux variation of cosmic muons", *arXiv preprint arXiv:1203.0101*, 2012.

[19] C. Nave, *Atmospheric muons*, http://hyperphysics.phy-astr.gsu.edu/hbase/hph.html, Accessed on 2018-08-13.

[20] CERN, *Cern neutrino platform*, https://home.cern/about/experiments/cern-neutrino-platform, Accessed on 2018-08-13.

[21] The ProtoDUNE-SP Collaboration, *Report on protodune-sp, np-04*, https://cds.cern.ch/record/2144868/files/SPSC-SR-185.pdf, Accessed on 2018-08-13.